International Journal of Biological Macromolecules 246 (2023) 125675

Contents lists available at ScienceDirect

International Journal of Biological Macromolecules

journal homepage: www.elsevier.com/locate/ijbiomac

Magnetic Fe_3O_4 nanoparticles loaded guava leaves powder impregnated into calcium alginate hydrogel beads (Fe_3O_4-GLP@CAB) for efficient removal of methylene blue dye from aqueous environment: Synthesis, characterization, and its adsorption performance

Venkata Subbaiah Munagapati [a], Hsin-Yu Wen [b], Anjani R.K. Gollakota [c,d], Jet-Chau Wen [a,d,*], Kun-Yi Andrew Lin [e], Chi-Min Shu [d], Vijaya Yarramuthi [f], Praveen Kumar Basivi [g], Guda Mallikarjuna Reddy [h,i], Grigory V. Zyryanov [h,j]

[a] Research Centre for Soil & Water Resources and Natural Disaster Prevention (SWAN), National Yunlin University of Science and Technology, Douliou, Yunlin 64002, Taiwan, ROC
[b] Department of Pathology, West China Hospital, Sichuan University, Chengdu 610041, PR China
[c] Department of Chemical and Materials Engineering, National Yunlin University of Science and Technology, Douliou, Yunlin 64002, Taiwan, ROC
[d] Department of Safety, Health, and Environmental Engineering, National Yunlin University of Science and Technology, Douliou, Yunlin 64002, Taiwan, ROC
[e] Department of Environmental Engineering, National Chung Hsing University, 250 Kuo-Kuang Road, Taichung, Taiwan, ROC
[f] Department of Chemistry, Vikrama Simhapuri University, Nellore 524320, Andhra Pradesh, India
[g] Pukyong National University Industry-University Cooperation Foundation, Pukyong National University, Busan 48513, Republic of Korea
[h] Chemical Engineering Institute, Ural Federal University, 620002 Yekaterinburg, Russian Federation
[i] Department of Chemistry, Sri Venkateswara University, Tirupati 517502, Andhra Pradesh, India
[j] Ural Division of the Russian Academy of Sciences, I. Ya. Postovskiy Institute of Organic Synthesis, 22 S. Kovalevskoy Street, Yekaterinburg, Russian Federation

ARTICLE INFO

Keywords:
Sodium alginate
Guava leaves powder
Magnetic hydrogel beads

ABSTRACT

In the present work, a novel Fe_3O_4-GLP@CAB was successfully synthesized via a co-precipitation procedure and applied for the removal of methylene blue (MB) from aqueous environment. The structural and physicochemical characteristics of the as-prepared materials were explored using a variety of characterization methods, including pH_{PZC}, XRD, VSM, FE-SEM/EDX, BJH/BET, and FTIR. The effects of several experimental factors on the uptake of MB using Fe_3O_4-GLP@CAB were examined through batch experiments. The highest MB dye removal efficiency of Fe_3O_4-GLP@CAB was obtained to be 95.2 % at pH 10.0. Adsorption equilibrium isotherm data at different temperatures showed an excellent agreement with the Langmuir model. The adsorption uptake of MB onto Fe_3O_4-GLP@CAB was determined as 136.7 mg/g at 298 K. The kinetic data were well-fitted by the pseudo-first-order model, indicating that physisorption mainly controlled it. Several thermodynamic variables derived from adsorption data, like as ΔG^o, ΔS^o, ΔH^o, and E_a, accounted for a favourable, spontaneous, exothermic, and physisorption process. Without seeing a substantial decline in adsorptive performance, the Fe_3O_4-GLP@CAB was employed for five regeneration cycles. Because they can be readily separated from wastewater after treatment, the synthesized Fe_3O_4-GLP@CAB was thus regarded as a highly recyclable and effective adsorbent for MB dye.

1. Introduction

The rapid development in science and technology profoundly revolutionized the industry sector. Nevertheless, this boost in industrial development also poses a toll on the ecosystem. One of the most vital examples of this kind is the contamination of water bodies due to effluents from the textile industry [1]. These effluents contain various recalcitrant compounds, toxic chemicals, and organic dyes that compromise aquatic life due to their toxic and carcinogenic nature [2–5]. Methylene Blue (MB) is a well-known synthetic thiazine cationic dye, heavily used in the textile industry to dye fabrics. Moreover, it is also being used in the paper and cosmetics industries for dyeing

* Corresponding author at: Research Centre for Soil & Water Resources and Natural Disaster Prevention (SWAN), National Yunlin University of Science and Technology, Douliou, Yunlin 64002, Taiwan, ROC.
E-mail address: wenjc@yuntech.edu.tw (J.-C. Wen).

https://doi.org/10.1016/j.ijbiomac.2023.125675
Received 26 April 2023; Received in revised form 28 June 2023; Accepted 1 July 2023
Available online 4 July 2023

purposes. However, exposure and accumulation of a significant amount of MB dye in the human body cause allergy, tissue necrosis, nausea, breathing difficulties, vomiting, skin irritation, mental confusion, and heart rhythm disturbances [6–9]. Therefore, it is pivotal to eliminate MB from the aqueous system using suitable removal methods.

In recent decades, several technologies, including bioremediation, advanced oxidation processes, photocatalytic degradation, ozonation, membrane filtering, solvent extraction, coagulation, and reverse osmosis, have been employed to remove dyes from wastewater [10]. Nevertheless, each of these therapeutic options has its own technical and commercial restrictions, such as expense, limited effectiveness, and toxicity caused by breakdown products. Nonetheless, the adsorption technique was assumed mainly owing to its simplicity, high efficiency, and operational flexibility. In this case, low-cost adsorbents like graphene oxide, activated carbon, and silica were used to remove refractory organic contaminants. Its uses, however, are severely limited because of the difficulties of separating after consumption, which may result in secondary water contamination. As a result, more efforts to investigate low cost, locally accessible, and valuable materials are required.

Several researchers have been carried out to evaluate the effectiveness of plant materials in eliminating potentially hazardous dyes from aqueous solutions [11–16]. *Psidium guajava* L. (the guava tree) belongs to the Myrtaceae family. The raw leaves contain various bioactive compounds such as tannins and flavonoids. Guava leaves are known for their medicinal value and have traditionally been used for different human ailments. Guava leaves contain various functional groups like ester, carboxylic acid, and hydroxyl, which can interact with and adsorb various pollutants [17]. These leaves are widely and almost freely available in every season of the year. Therefore, guava leaf powder has been used as a starting material in its native form in the current study. Nevertheless, the use of plant materials as biosorbents in their natural form also suffers from limitations like low specific surface area, leaching of selective adsorbent components into treated water, low adsorption efficiency, and difficulty in removing the adsorbent compound after the adsorption process [18]. Therefore, magnetic sorbents such as magnetite iron oxide nanoparticles (Fe_3O_4) were used in agricultural waste to overcome these limitations. These nanoparticles increase the surface area, reactivity, adsorption efficacy, and reusability but at the same time decrease the intraparticle diffusion rate. Moreover, due to the paramagnetic property, the iron oxide nanoparticles can be easily removed from the aqueous environment after their usage by simply exposing them to the external magnetic field [19,20]. Numerous researchers have evaluated the use of Fe_3O_4 nanoparticles coated biomass as a biosorbent for potentially toxic dye remediation [21–25].

Sodium alginate is a linear biopolymer known to be a widely used adsorbent. This adsorbent possesses carboxyl and hydroxyl functional groups that help the alginate to form complexes with various multivalent ions leading to increased affinity and adsorptive capacity towards different pollutants [26]. Moreover, alginate is a biodegradable and abundant polymer available in nature. Due to these, it is a low cost and eco-friendly sorbent [27]. Therefore, calcium alginate is often used to encapsulate a variety of nanomaterials, including magnetic nanoparticles is a sophisticated method to minimize loss of mass and overcome the enormous waste generated after treatment [28]. This will also assist lower the cost of regeneration and large scale water treatment.

To the best of our knowledge, there has been no research on using Fe_3O_4-GLP@CAB as an adsorbent for removing MB dye. Thus in this study, Fe_3O_4-GLP@CAB was synthesized, characterized, and employed as a sorbent to eliminate MB. The removal of MB by Fe_3O_4-GLP@CAB and the recovery of the dye from the adsorbent were carried out. Parameters impacting MB dye removal efficiencies like MB dye concentration, Fe_3O_4-GLP@CAB dosage, agitation speed, adsorption duration, temperature, and solution pH were considered. Thermodynamic, isotherm, and kinetic data were evaluated to explore the sorption mechanism. The goal of this effort is to develop a perfect biosorbent that can: (i) demonstrate a significant affinity for MB dye; (ii) be readily removed from the solution after treatment; and (iii) be easily and frequently recycled.

2. Materials and methods

2.1. Chemicals

MB dye (molecular mass: 319.85 g/mol, formula: $C_{16}H_{18}N_3SCl$, λ_{max}: 665 nm), $CaCl_2$ (calcium chloride), $FeSO_4.7H_2O$ (iron (II) sulfate heptahydrate), NaOH (sodium hydroxide), $FeCl_3.6H_2O$ (iron (III) chloride hexahydrate), HCl (hydrochloric acid), C_2H_6O (ethanol), and $C_6H_7O_6Na$ (sodium alginate) were all acquired from Sigma-Aldrich. All the reagents utilized in this investigation were of analytical purity and weren't purified before use. Deionized (DI) water was used to make each dilution.

2.2. Synthesis of the Fe_3O_4-GLP@CAB

Fresh green leaves of guava were gathered locally and washed frequently with DI water to eliminate dust particles and other adherent contaminants on the surface. The clean and dust-free leaves were first sun-dried for 2–3 days and then allowed to dry in an oven at 343 K for 10 h. After that, the dried leaves were grounded into a fine powder using a mechanical grinder and then passed through 30 mesh sieves. The obtained product is labeled as guava leaves powder (GLP).

The Fe_3O_4-GLP composite was synthesized by a co-precipitation procedure [10]. During this process, an amount of 10 g GLP was added into a 400 mL solution containing $FeSO_4.7H_2O$ (3.80 g) and $FeCl_3.6H_2O$ (7.80 g). For 60 min, the aforesaid mixture was constantly mixed at 343 K. To precipitate Fe_3O_4 nanoparticles, NaOH solution (5.0 M) was added dropwise to the reaction mixture until the pH reached 10.0–11.0. The mixture was rapidly agitated for 60 min at 343 K before maturing for 24 h at 298 K. After removing the black residue from the solution using an external magnetic field, the solution was washed repeatedly with DI water and ethanol until the pH approached neutral. The rinsed product (Fe_3O_4-GLP) was dried at 343 K in an oven for 24 h.

In a typical procedure, sodium alginate (3 %) was dissolved in DI water for 4 h at room temperature by stirring until complete dissolution. The required quantity (1.0 g) of Fe_3O_4-GLP was then infused into the gel solution. To prevent the production of air bubbles within the viscous liquor, the solution was gently swirled for 24 h. The mixture was then dropped gradually into a 4 % aqueous solution of $CaCl_2$ using a micropipette tip (1.0 mL). Hence, spherical polymer beads were created right away. In fact, the exchange of Na for Ca cations causes cross-linkages in the alginate polymer chains, which leads to the formation of the beads [29]. The produced beads were left in the $CaCl_2$ solution for 12 h. The beads were then extracted from the solution using an external magnetic field before being repeatedly rinsed in DI water to eliminate any calcium and free (unreacted) alginate. The produced hydrogel beads (Fe_3O_4-GLP@CAB) were stored in DI water in an airtight plastic recipient for further use. The procedure for preparing the Fe_3O_4-GLP@CAB is schematically given in Fig. 1.

2.3. Instrumentation

Field emission scanning electron microscopy (FESEM; JSM7610F; JEOL; Japan) at 5.0 kV scanning voltages, with an accelerating voltage of 20 kV, was used to investigate the morphologies of the samples. In contrast, energy dispersive X-ray spectroscopy (EDX; Oxford Instruments; UK) was used to determine elemental composition. The structure and crystallinity of the materials were examined by X-ray diffraction (XRD; D8 Advance; Bruker AXS GmbH; Germany) equipped with Cu/Kα radiation ($\lambda = 1.542$ Å) at 2θ angular range of 10-80°. The magnetic characteristics of the synthesized nanocomposites were measured in a range of ±20 KOe using a vibrating sample magnetometer (VSM; Quantum Design; MPMS3; USA) at 298 K. Fourier transform infrared (FTIR; Thermo Nicolet iS10; USA) spectroscopy in the

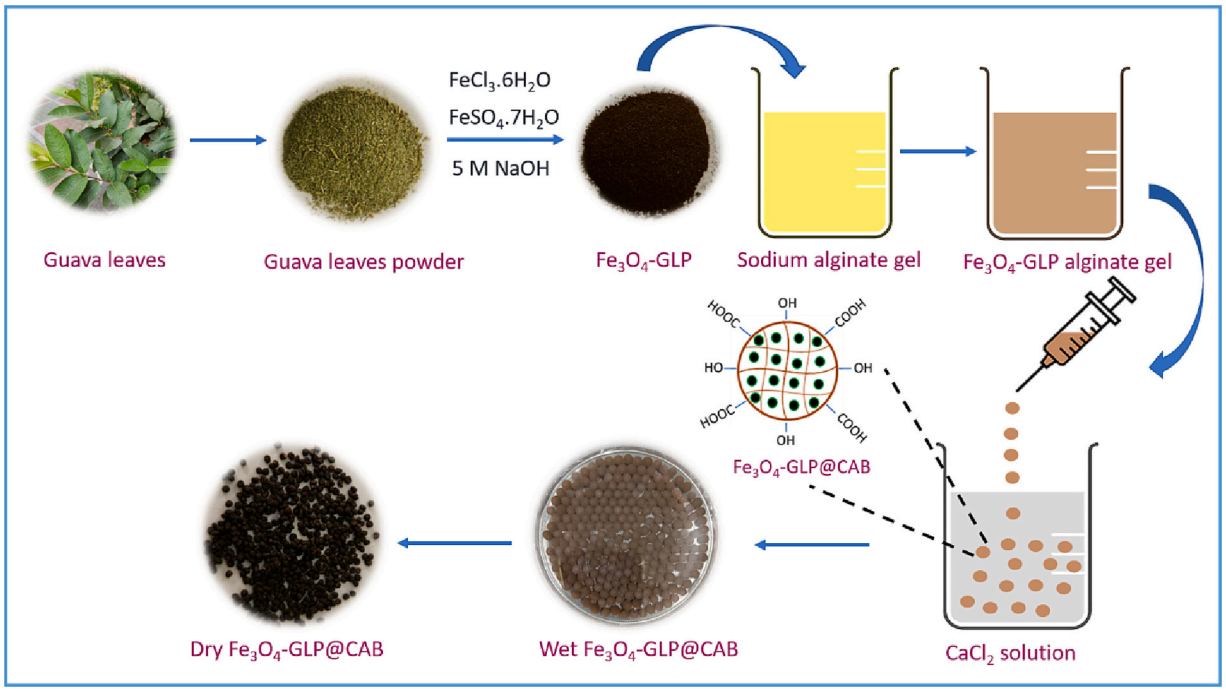

Fig. 1. Schematic diagram of the synthesis of Fe_3O_4-GLP@CAB.

400–4000 cm^{-1} range with a resolution of 2.0 cm^{-1} in KBr pressed pellet at 298 K identified the surface functional groups of the synthesized samples. The pore radius and pore volume were determined by the BJH (Barrett Joyner Halenda) model using a specific surface area analyzer (Quantachrome; Autosorb-iQ; USA) at 77 K with relative pressure range of 0.01–0.999. N_2 isotherms (adsorption and desorption) were used to determine the surface area of the materials according to the BET (Brunauer Emmett Teller) model. The pH meter (Thermo Orion Star A214; USA) was used to measure the pH value of MB solutions. A UV/Vis (V-750; JASCO; Japan) spectrophotometer with a maximum wavelength of 665 nm was used to analyze the sample concentrations according to standard procedures.

2.4. Adsorption experiments

1.43 g of the MB dye was dissolved in 1.0 L of DI water to make a 1000 mg/L stock solution. The stock solution was used to set up the distinctive working solutions. Batch tests were performed in a temperature-controlled orbital shaking incubator using 50 mL glass vials containing 30 mL of working solutions. Different adsorption parameters, for instance, pH (2.0–11.0), dosage (0.2–1.6 g/30 mL), MB dye concentration (25, 50, 75, 100, 125, 175, and 250 mg/L), contact duration (0–300 min), stirring speed (50–350 rpm), and temperature (298–333 K) were examined to determine their impact on the removal of MB onto Fe_3O_4-GLP@CAB. The adsorption isotherms experiments were performed separately at diverse MB dye concentrations (25–250 mg/L) under 298, 308, 318, and 328 K. Furthermore, for various contact duration (0–300 min), the adsorption kinetics of Fe_3O_4-GLP@CAB was studied at an MB dye concentration of 25 mg/L at 298 K respectively. The pH of working solutions has been attuned by using NaOH and HCl solutions (0.1 M). After adsorption equilibrium, the Fe_3O_4-GLP@CAB was separated from the adsorbate by an external magnet. A UV–Vis spectrophotometer measured the MB dye concentration in the remaining solution. Each test was repeated twice, presenting their average as the final results. The removal percentage R (%), and adsorption uptake, q_e (mg/g) of the MB on Fe_3O_4-GLP@CAB was calculated using Eqs. (1) & (2), respectively.

$$R = \left(\frac{C_o - C_e}{C_o}\right) \times 100\% \quad (1)$$

$$q_e = \frac{(C_o - C_e)\, V}{M} \quad (2)$$

where C_o (mg/L) and C_e (mg/L) are the concentrations of MB dye in their initial and equilibrium states, respectively. M (g) is the weight of the Fe_3O_4-GLP@CAB, and V (mL) is the volume of the MB solution.

2.5. Desorption and reusability

Five different desorbing eluents (DI water, 0.2 M HNO_3, 0.2 M NaOH, 0.2 M $(CH_3)_2CO$, and 0.2 M C_2H_5OH) were used to investigate the desorption of MB from Fe_3O_4-GLP@CAB. For this purpose, after performing adsorption tests using Fe_3O_4-GLP@CAB under optimal conditions, a magnet separated the spent sorbent from the liquid phase. It was then placed in various desorption eluents (30 mL) under an orbital shaker at 250 rpm for 90 min. The Fe_3O_4-GLP@CAB was separated after agitation, and the dye concentration in the adsorbate was evaluated using a UV–Vis spectrophotometer. The Fe_3O_4-GLP@CAB were cleaned with DI water and dried to explore their reusability. Five cycles of cyclic adsorption/regeneration were investigated. After each cycle, the reusability of Fe_3O_4-GLP@CAB was determined. The % of desorption was calculated using Eq. (3):

$$Desorption\ (\%) = \frac{Dye\ \text{desorbed}}{Dye\ \text{adsorbed}}\ X\ 100 \quad (3)$$

2.6. Statistical analysis

The suitable models that fit the experimental data were selected based on kinetic and isotherm studies, non-linear regression analysis, and the values of the correlation coefficient (R^2) as well as the error functions, such as the SSE (sum of squares) and the χ^2 (mean square), for which the calculation equations are provided below. The related model's goodness of fit is shown by high R^2, lower SSE, and χ^2 values.

$$\chi^2 = \sum_{i=1}^{n} \left(\frac{(q_{e,exp} - q_{e,cal})^2}{q_{e,cal}} \right) \quad (4)$$

$$SSE = \sum_{i=1}^{n} (q_{e,cal} - q_{e,exp})^2 \quad (5)$$

where $q_{e,\,cal}$ is the calculated quantity sorbed given by the model, $q_{e,\,exp}$ is the experimental quantity sorbed at equilibrium, and n is the number of observations.

3. Results and discussion

3.1. Characterization (FTIR, FE-SEM/EDX, VSM, XRD, BET-BJH, and pH_{PZC})

FTIR spectroscopy is often used to recognize the functional groups on a surface, and functional groups play a crucial role in the dye sorption process. FTIR spectra of GLP, Fe_3O_4-GLP, CAB, Fe_3O_4-GLP@CAB, and MB dye-loaded Fe_3O_4-GLP@CAB were shown in Fig. 2. In the spectrum of GLP (Fig. 2a), the intense peak at 3284 cm^{-1} which corresponds to the stretching vibration of hydrogen-bonded alcoholic and phenolic –OH groups in GLP [30,31]. The 2916 and 2847 cm^{-1} peaks were related to C—H stretching vibrations from–CH_3/-CH_2/-CH in hemicellulose, lignin, and cellulose, respectively [32]. The band at 1733 cm^{-1} could be assigned to the stretching vibration of C═O groups like carboxylic acids, ketones, and aldehydes. The peak at 1626 cm^{-1} can be attributed to the stretching vibration of -C═O bond in carbonyl group [33,34]. The peak at 1540 cm^{-1} was assigned to alkanes' –C═C- stretching vibrations. The 1440 and 1370 cm^{-1} peaks were attributed to C═C (aromatic ring) and –C-H stretching vibrations of the lignin structure in GLP [35]. The peaks at 1313 and 1029 cm^{-1} corresponded to the C—O and C-O-C stretching of cellulose present in GLP. The band at 1236 cm^{-1} belongs to the C—O stretching vibration of the acetyl group in hemicelluloses [32]. In the spectrum of Fe_3O_4-GLP (Fig. 2b), some peaks in GLP disappeared (2916, 2847, 1733, 1540, 1440, 1370, 1236 cm^{-1}), and some peaks are at 3284, 1626, 1313, and 1029 cm^{-1} were slightly shifted to 3361, 1629, 1318, and 1065 cm^{-1}. The sharp peak observed at 551 cm^{-1} corresponds to the stretching of Fe—O bonds in the crystalline lattice of Fe_3O_4 [36]. This characteristic band confirms the Fe_3O_4 nanoparticles were successfully loaded in the GLP. For CA B (Fig. 2c), the peak at 3267 cm^{-1} is related to the –OH stretching vibrations of the hydroxyl groups of calcium alginate [37]. The absorption peaks appearing near 1590 and 1411 cm^{-1} were associated with symmetric and asymmetric stretching of the carboxylate ($-COO^-$) groups of Ca-alginate, respectively [38]. The peak at 1018 cm^{-1} is identified as a characteristic peak for the –C-O and –C-O-C stretching on polysaccharides [18]. FTIR spectrum of Fe_3O_4-GLP@CAB (Fig. 2d), the peak observed at 3281 cm^{-1} corresponding to the -OH groups of carboxylic acid [39]. The peaks around at 2923, 2849, and 1034 cm^{-1} are the symmetric, asymmetric stretching of –CH_2 groups and C-O-C stretching vibrations, respectively [36]. The absorption band at 1710 cm^{-1} can be assigned to the carboxylate groups bonded onto the surface of Fe_3O_4-GLP@CAB. The band at 1633 cm^{-1} corresponded to the stretching vibrations of the C═O group. The peaks at 1536 and 1409 cm^{-1} correspond to $–COO^-$ symmetric & asymmetric stretching vibrations [29]. The band at 1239 cm^{-1} is attributed to the stretching of the C—O group. The peak at 546 cm^{-1} represented the characteristic stretching of Fe—O from nanoparticles of Fe_3O_4-GLP. However, all the absorption peaks confirmed that the Fe_3O_4-GLP nanoparticles were successfully incorporated into the sodium alginate beads. The FTIR spectrum of MB dye-loaded Fe_3O_4-GLP@CAB (Fig. 2e) gave similar characteristic peaks to those that appeared for Fe_3O_4-GLP@CAB; however, the peaks at 3281, 2923, 2849, 1633, 1409, 1034, 546 cm^{-1} were slightly shifted to 3220, 2921, 2848, 1636, 1430, 1048, and 568 cm^{-1}, respectively. Three bands at 1710, 1536, and 1239 cm^{-1} disappeared after dye adsorption. These changes indicated the strong interactions between the Fe_3O_4-GLP@CAB and MB dye through hydrogen bonding or electrostatic interactions.

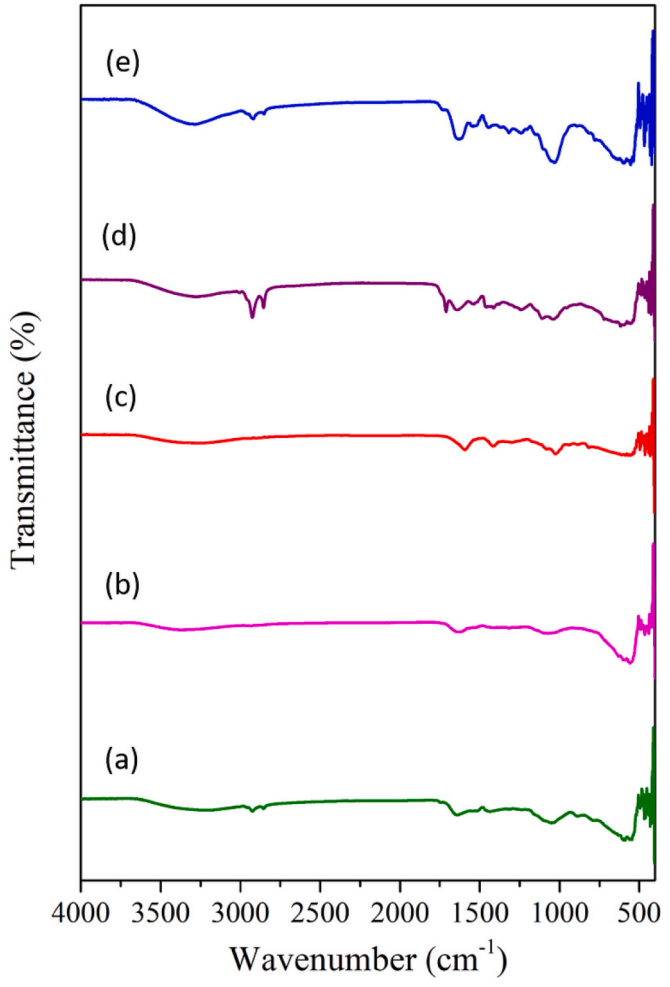

Fig. 2. FTIR images of (a) GLP, (b) Fe_3O_4-GLP, (c) CAB, (d) Fe_3O_4-GLP@CAB, (e) MB/Fe_3O_4-GLP@CAB.

The magnetic properties of Fe_3O_4-GLP and Fe_3O_4-GLP@CAB were determined by the VSM, where the obtained magnetic hysteresis loops are depicted in Fig. 3. The Ms. (saturation magnetization) of Fe_3O_4-GLP

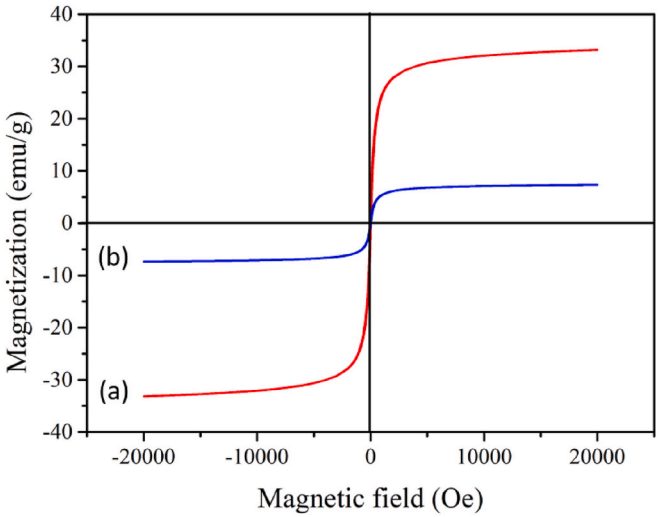

Fig. 3. Magnetic hysteresis curves of (a) Fe_3O_4-GLP and (b) Fe_3O_4-GLP@CAB.

was 35.1 emu/g while Fe_3O_4-GLP@CAB was 7.8 emu/g. Compared to Fe_3O_4-GLP, this decrease in the magnetic properties of Fe_3O_4-GLP@CAB was due to the presence of a non-magnetic substance (Ca-alginate) on the surface of magnetic particles [40]. However, the magnetism of the Fe_3O_4-GLP@CAB was sufficient for fast separation and reuse using an external magnetic field.

The FE-SEM/EDX analysis provides information about the morphology of the surface and the composition of elements of the materials. FE-SEM images of GLP, Fe_3O_4-GLP, CAB, Fe_3O_4-GLP@CAB, and MB dye-loaded Fe_3O_4-GLP@CAB are shown in Fig. 4. The GLP had an irregular and smooth surface morphology (Fig. 4a). After loading Fe_3O_4 particles in GLP (Fig. 4b) the surface morphology was converted to be rougher, irregular, and heterogeneous. The external shape of the CAB, Fe_3O_4-GLP@CAB, and MB-loaded Fe_3O_4-GLP@CAB was spherical (Fig. 4c, d, and e). The CAB had a relatively smooth surface, whereas the Fe_3O_4-GLP@CAB surface was rougher due to incorporating Fe_3O_4-GLP particles into the CAB. The surface roughness plays a significant role in dye ions binding since it enhances the contact area, which made the surface easier for dye sorption. After MB adsorption, the surface of the Fe_3O_4-GLP@CAB became smoother because MB dye molecules covered the surface of the Fe_3O_4-GLP@CAB. The EDX spectrum and elemental composition data of GLP, Fe_3O_4-GLP, CAB, Fe_3O_4-GLP@CAB, and MB dye-loaded Fe_3O_4-GLP@CAB are shown in Fig. 5. The EDX spectrum of GLP as seen in Fig. 5a that displays the presence of C, O, Mg, S, Cl, K and Ca. The EDX spectrum of GLP-Fe_3O_4 reveals the presence of C, O, Na, S, Cl, and Fe elements. The existence of a new Fe peak in the spectrum (Fig. 5b), which confirmed the deposition of Fe_3O_4 nanoparticles on the GLP surface. The O, Na, Cl, and Ca were the major elements observed in the EDX spectrum of CAB (Fig. 5c). The EDX spectrum of Fe_3O_4-GLP@CAB contained elements of C, O, Al, Si, Ca, and Fe (Fig. 5d). Compared to the CAB spectrum, the new C, Si, and Fe peaks appeared in the spectrum of Fe_3O_4-GLP@CAB, which confirms the successful incorporation of Fe_3O_4-GLP particles into the CAB. The S peak was observed in the EDX spectrum of MB dye-loaded Fe_3O_4-GLP@CAB (Fig. 5e), which confirmed that the MB dye was bound onto the Fe_3O_4-GLP@CAB surface after the adsorption process.

One of the primary techniques for examining crystal structure and identifying phases is X-ray diffraction analysis. Fig. 6 presents the XRD patterns of the GLP, Fe_3O_4-GLP, CAB, and Fe_3O_4-GLP@CAB. The XRD patterns of GLP (Fig. 6a) show the presence of a set of peaks at an angular position at 15.1°, 21.3°, and 30.1° & 38.4°. The diffraction peak of GLP at 2θ around 15.1° was assigned to the crystalline plane of (110) for cellulose and those at 2θ = 21.3°, and 30.1° & 38.4° were attributed to the crystalline planes of (200) and (004), respectively, which attributed to the typical cellulose [41]. The XRD pattern of the Fe_3O_4-GLP composite (Fig. 6b) showed characteristic diffraction peaks at 2θ values of 30.6°, 35.9°, 43.7°, 54.1°, 57.4°, and 63.1°, corresponding to the crystal planes of (220), (311), (400), (442), (511), and (440), respectively. Both angular positions and intensity of these summits were very well-matched with the standard JCPDS file No. 19–06290 of magnetite (Fe_3O_4) [42]. The Fe_3O_4-GLP diffraction peaks confirmed that the Fe_3O_4 nanoparticles were successfully loaded in the GLP. The XRD pattern of the pure CAB displays three weak diffraction peaks at 2θ = 13.5°, 21.5°, and 38.8° without any other prominent sharp diffraction peak (Fig. 6c), which indicates the semi-crystallinity of the biopolymer [43]. The XRD pattern of Fe_3O_4-GLP@CAB material (Fig. 6d) displays that major diffraction peaks are in the same position as the synthesized Fe_3O_4-GLP composite but with a slightly lower intensity, which indicates the successful incorporation of Fe_3O_4-GLP particles inside alginate hydrogel beads.

The adsorbent's porosity and specific surface area significantly impact its adsorption characteristics, which may give critical information on sorption properties. As a result, it is critical to assess structural factors such as surface area and porosity using the BET adsorption technique. The Fe_3O_4-GLP@CAB BJH and N_2 adsorption-desorption plots (Fig. 7) matched with the type-IV diagram in the IUPAC classification, indicating a mesoporous structure. On the basis of N_2 isotherm (adsorption/desorption) and BJH pore size distribution, the values of surface area, pore radius, and pore volume of GLP, Fe_3O_4-GLP, CAB, and Fe_3O_4-GLP@CAB were determined and listed in Table 1. From Table 1, the surface area of GLP was 6.79 m^2/g. After Fe_3O_4 modification, the surface area of Fe_3O_4-GLP was significantly increased to 62.81 m^2/g (9.3

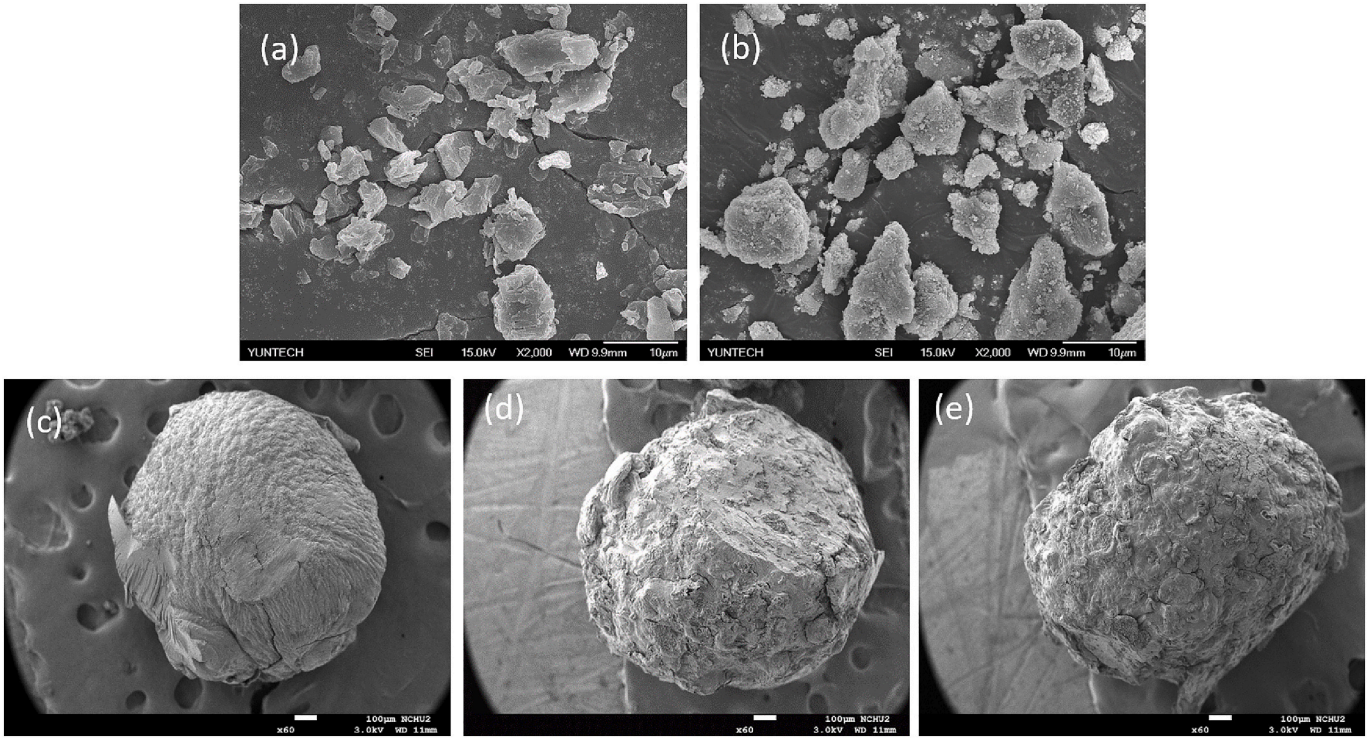

Fig. 4. FE-SEM images of (a) GLP, (b) Fe_3O_4-GLP, (c) CAB, (d) Fe_3O_4-GLP@CAB, (d) MB/Fe_3O_4-GLP@CAB.

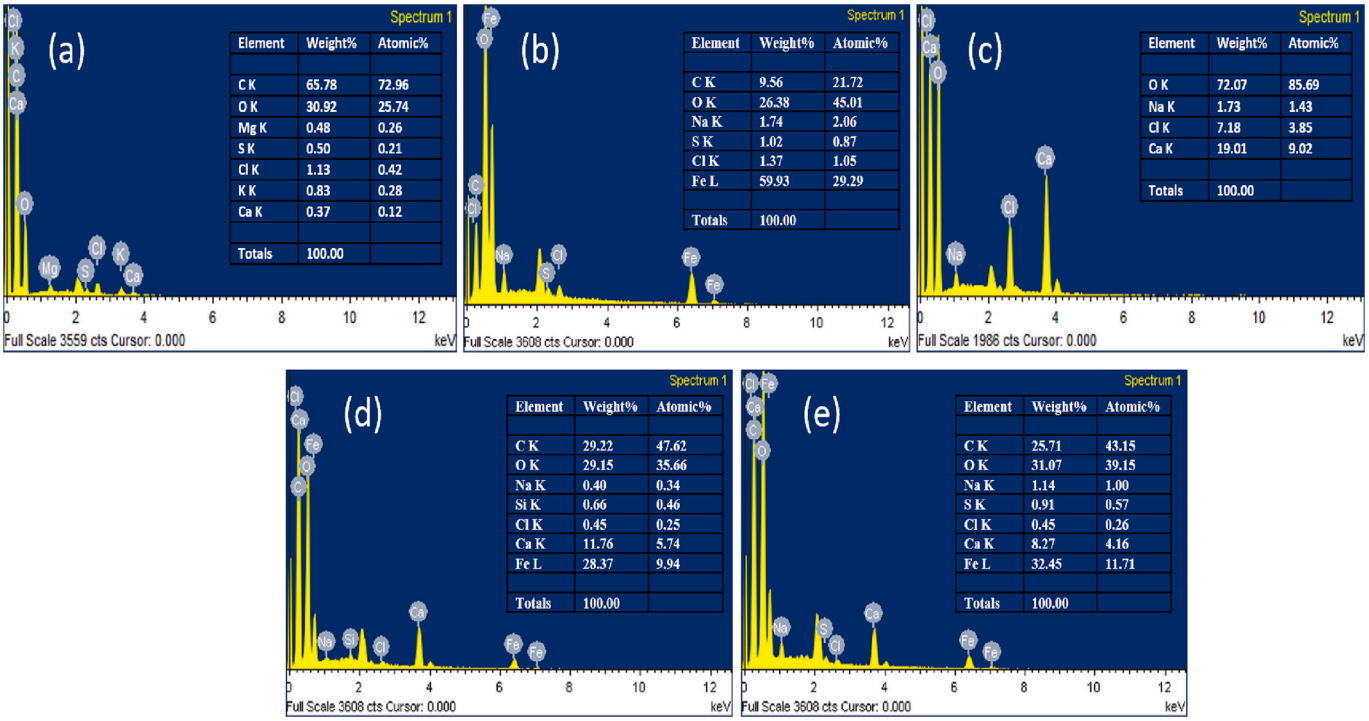

Fig. 5. EDX images of (a) GLP, (b) Fe_3O_4-GLP, (c) CAB, (d) Fe_3O_4-GLP@CAB, (d) MB/Fe_3O_4-GLP@CAB.

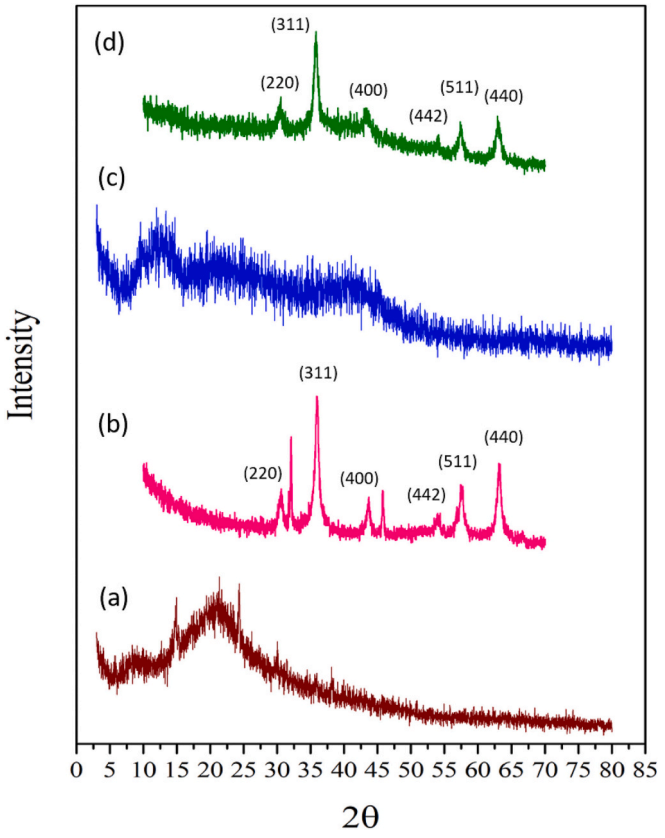

Fig. 6. XRD pattern of (a) GLP, (b) Fe_3O_4-GLP, (c) CAB, (d) Fe_3O_4-GLP@CAB.

times higher), primarily attributed to forming Fe_3O_4 particles [44]. Introducing Fe_3O_4-GLP nanoparticles into CAB leads to Fe_3O_4-GLP@CAB with a higher BET surface area than pure CAB, which is attributed to the cracks due to Fe_3O_4-GLP inclusion, and therefore, Fe_3O_4-GLP@CAB could improve the beads' ability to adsorb pollutants [45]. The surface area of Fe_3O_4-GLP@CAB is less than that of the Fe_3O_4-GLP composite encapsulated in the CAB because alginate occupies the mesoporous of Fe_3O_4-GLP. However, the Fe_3O_4-GLP@CAB has a good surface area, pore volume, and pore radius has a strong adsorption uptake for MB, which will be very beneficial in water treatment.

The pH_{PZC} (point of zero charge) of Fe_3O_4-GLP@CAB was determined by using the solid addition procedure [10]. For that, 0.01 M solution of NaCl (30 mL) in 50 mL glass vials was adjusted to different pH values of 2.0–11.0 (initial pH) using HCl and NaOH (0.1 M) solutions. After, an exact amount of 1.0 g of Fe_3O_4-GLP@CAB was added to different vials and kept at 250 rpm in an orbital shaking incubator at 298 K for 24 h. Following incubation, the pH of each vial was measured and recorded as the final pH. The variance between the initial and final pH values was calculated and plotted against the initial pH values (ΔpH = final pH-initial pH). The pH_{PZC} value may be calculated by plotting the curves when the pH is zero and intersecting them with the X-axis (Fig. S1).

3.2. Effect of pH, initial MB dye concentration, agitation speed, Fe_3O_4-GLP@CAB dosage, and contact duration

The pH of the MB solution obviously influences the sorption efficiency of the Fe_3O_4-GLP@CAB. So, the impact of pH value on the MB adsorption process was studied in the pH value range from 2.0 to 11.0.0.1 M NaOH/HCl solutions were used to adjust the pH of the dye solutions. As seen from Fig. 8a, the removal efficiency of MB raised from 12.9 to 95.2 % with an increase in pH values from 2.0 to 10.0, after that the removal efficiency was almost constant. This tendency mainly depends on the electrostatic interaction between the MB dye and Fe_3O_4-GLP@CAB. The higher removal efficiency of MB on Fe_3O_4-GLP@CAB was found at pH 10.0. The pKa value of MB dye is 3.8. The MB dye molecule dissociates at pH > pKa while remaining in its molecular state at pH < pKa. The pH_{PZC} of Fe_3O_4-GLP@CAB was 6.8. At pH below pH_{PZC}, the Fe_3O_4-GLP@CAB surface is +vely charged (X-OH_2^+, X-$COOH_2^+$) owing to an abundance of H^+ ions which promotes electrostatic repulsion between the cationic MB dye and the Fe_3O_4-GLP@CAB,

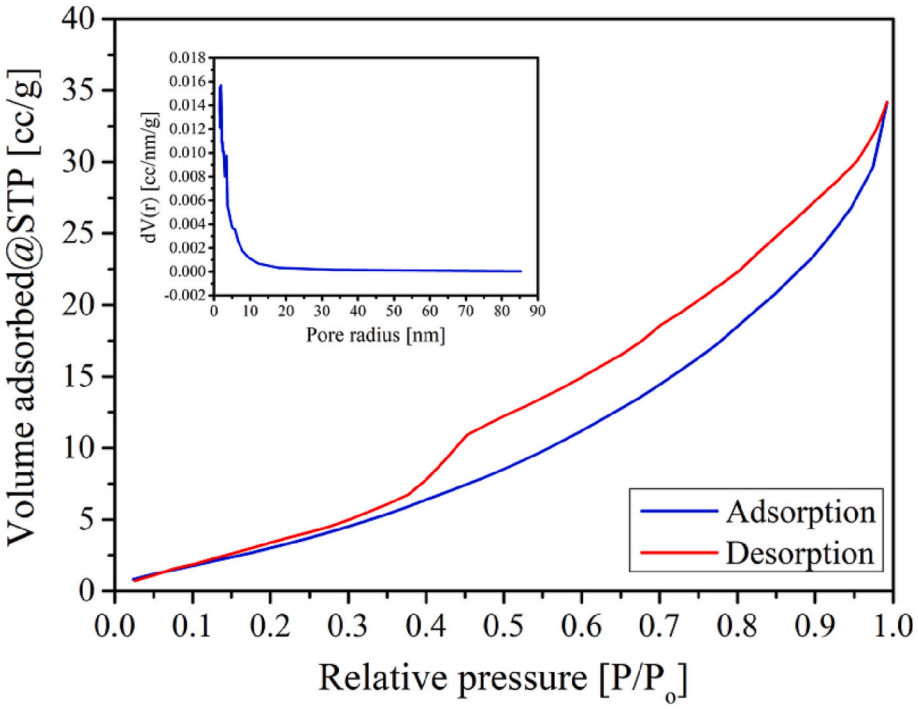

Fig. 7. BET N_2 adsorption-desorption isotherm and inset BJH pore size distribution plots of Fe_3O_4-GLP@CAB.

Table 1
Textural properties of the prepared adsorbents.

Adsorbent	BET Surface area (m^2/g)	Pore volume (cc/g)	Pore radius (nm)
GLP	6.79	0.0087	1.5773
Fe_3O_4-GLP	62.81	0.1782	1.7127
CAB	1.11	0.0092	1.4921
Fe_3O_4-GLP@CAB	27.97	0.0529	2.1663

therefore resulting in low removal efficiency. At pH above pH_{PZC}, the Fe_3O_4-GLP@CAB surface was –vely charged and the MB dye was dissociated, and the removal efficiency increased due to deprotonation of the functional sites at the Fe_3O_4-GLP@CAB surface ($X\text{-}O^-$, $X\text{-}COO^-$), resulting in a more –vely charged surface, attracting the MB cations more efficiently than at lower pH of the solution. Thus, the movement of MB cations towards the –vely charged Fe_3O_4-GLP@CAB was facilitated by electrostatic interaction. Similar findings have been observed in previously published literature when the removal of the MB has been investigated [46–48]. Based on the findings, 10.0 was fixed as the optimal solution pH for all the subsequent adsorption experiments.

The influence of the initial dye concentration on the removal of MB by the Fe_3O_4-GLP@CAB was examined by changing the concentration from 25 to 250 mg/L at 298 K. As displayed in Fig. 8b, the removal effectiveness of MB declined steadily from 95.1 to 52.3 % when the starting concentration raised from 25 to 250 m/L. This may be attributed to the adsorbent's restricted number of active sites as the solute concentration rises. Generally, the sorption process is primarily monolayer at low starting dye concentrations, which is then expanded to multilayer until the equilibrium stage is attained at high solute concentrations. Furthermore, at high dye concentrations, the driving power needed is more significant to overcome the mass transfer barrier of solute molecules between the solid and liquid stages [49]. The maximal removal efficiency of MB dye was found at 25 mg/L; hence all the further tests were conducted using a concentration of 25 mg/L.

Agitation speed is a significant factor in the sorption process which influences the distribution of the solute and adsorbent in the bulk solution. The impact of agitation speed on the removal of MB by Fe_3O_4-GLP@CAB was tested at various stirring speeds ranging from 50 to 350 rpm, as shown in Fig. 8c. The results revealed an increase in agitation speed, the removal effectiveness rose up to 250 rpm. Therefore, it was hypothesized that with the rise in agitation speed, the randomness of the dye molecules increased and got efficiently adsorbed onto the pores of the Fe_3O_4-GLP@CAB. Further increase in agitation speed had no influence on the removal percentage, which suggested the occupancy of all the surface pores of Fe_3O_4-GLP@CAB and steric hindrance of adsorbed dye molecules with the unadsorbed ones [50]. Thus, 250 rpm was considered the optimum speed and maintained for further study.

The adsorbent dose is a crucial element in an adsorption process and significantly impacts the rate of dye removal. By varying the quantity of sorbent from 0.2 to 1.6 g, as shown in Fig. 8d, the effect of Fe_3O_4-GLP@CAB dose on the removal efficiency of MB dye was examined. It was shown that, up to 1.0 g of adsorbent, the percentage of dye removal initially rises with an increase in Fe_3O_4-GLP@CAB quantity; however, beyond this dose, the removal percentage stays relatively constant. This is explained by the fact that when adsorbent doses rise, more accessible adsorption sites become available. It was noticed that beyond 1.0 g, there were no appreciable changes in adsorption capabilities. Additionally, using adsorbent in excess or outside of recommended limits might cause dye molecules to aggregate at accessible adsorbent sites or result in an unpleasant interaction between the dye and adsorbent [51]. Based on the above results, the maximal removal efficiency of up to 95.2 % was achieved at a 1.0 g/30 mL dosage which can be considered an optimum dosage for further studies.

The contact period between the adsorbent and the adsorbate is a crucial variable for determining the effectiveness of a sorption process, especially at the industrial scale. The impact of MB adsorption contact time on the Fe_3O_4-GLP@CAB was studied from 0 to 300 min at 25 mg/L. As demonstrated in Fig. 8e, the dye removal efficiency was initially quick, then decreased until equilibrium. Initially, more binding moiety sites for dye ions binding were present, so the dye was removed fast at the start, resulting in a rapid dye capacity. Alternatively, as the reaction time advances, the active binding sites become occupied, resulting in competition for remaining dye molecules; as a consequence, dye

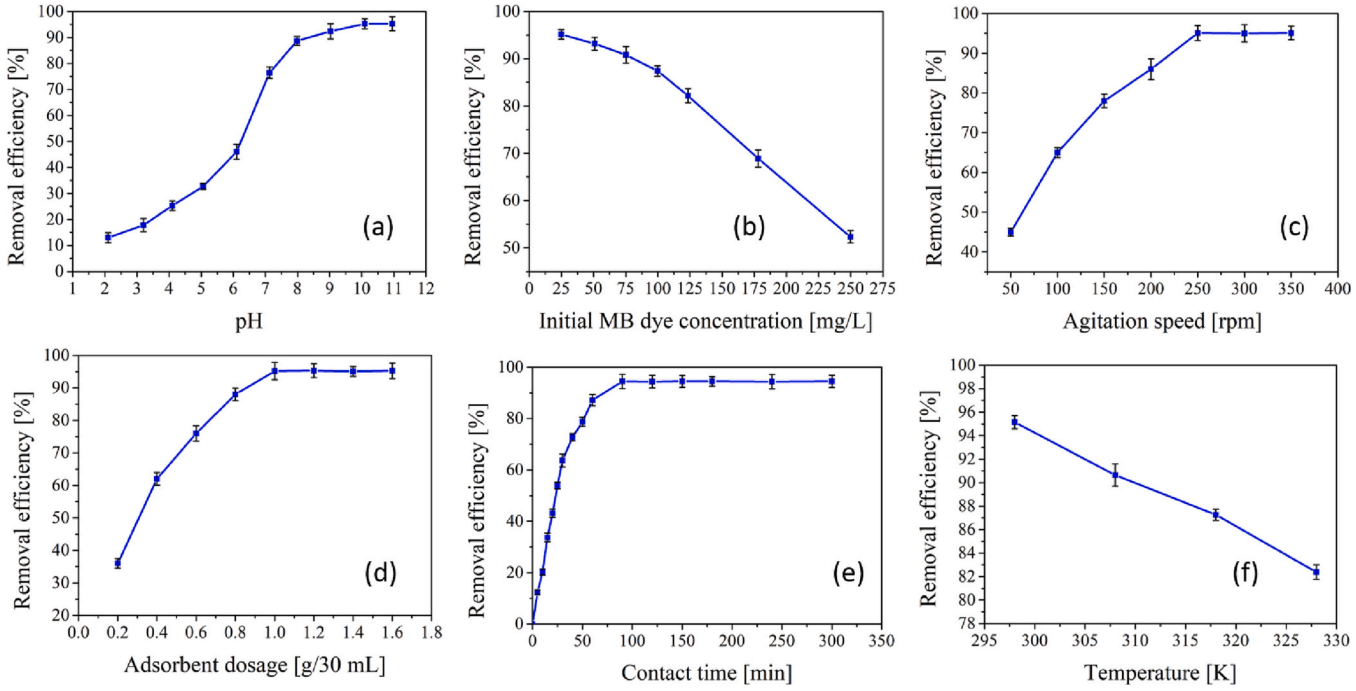

Fig. 8. Effect of various parameters for adsorption of MB on Fe_3O_4-GLP@CAB (a) effect of pH [pH = 2.0–11, C_o = 25 mg/L, time = 90 min, volume = 30 mL, dosage = 1.0 g, speed = 250 rpm, T = 298 K] (b) initial MB dye concentration [C_o = 25–250 mg/L, pH = 10, dosage = 1.0 g, time = 90 min, volume = 30 mL, speed = 250 rpm, T = 298 K] (c) stirring speed [speed = 50–350 rpm, pH = 10, time = 90 min, C_o = 25 mg/L, dosage = 1.0 g, volume = 30 mL, T = 298 K] (d) dosage [dosage = 0.2–1.6 g, C_o = 25 mg/L, time = 90 min, volume = 30 mL, speed = 250 rpm, T = 298 K] (e) contact duration [time = 0–300 min, C_o = 25 mg/L, dosage = 1.0 g, volume = 30 mL, speed = 250 rpm, T = 298 K] (f) temperature [T = 298–328 K, C_o = 25 mg/L, speed = 250 rpm, time = 90 min, dosage = 1.0 g, volume = 30 mL].

removal was hampered later on [52]. The equilibrium time was attained in 90 min, and no substantial change was detected after that. As a result, 90 min was identified as the optimal contact duration for further research. The results of this study are used to compute the kinetic factors of adsorption and predict the characteristics of the sorption process.

3.3. Adsorption kinetics

The kinetic analysis of the sorption experiment is critical and deserving of attention in order to categorize the sorption rate, reaction pathway, effectiveness of the sorbent, and reaction rate of the system. The kinetic evaluation of the adsorption of MB by Fe_3O_4-GLP@CAB has been performed by fitting the equilibrium data into well-known PFO (pseudo-first-order), PSO (pseudo-second-order), and Elovich models. PFO, PSO, and Elovich model non-linear equations are represented as follows:

$$q_t = q_e\left(1 - e^{-k_1 t}\right) \tag{6}$$

$$q_t = \frac{q_e^2 k_2 t}{1 + q_e k_2 t} \tag{7}$$

$$q_t = \frac{1}{\beta} ln(1 + \alpha\beta t) \tag{8}$$

where q_t (mg/g) and q_e (mg/g) are the quantities of MB adsorbed at equilibrium and at time t, respectively. k_2 (g/mg min) and k_1 (1/min) are the reaction rate constants of PSO and PFO, respectively. α (mg/g min) is the starting rate of adsorption, and β (g/mg) is the constant of desorption. The fitting findings of non-linearized PSO, PFO, and Elovich models are depicted in Fig. 9, and the recovered variables evaluated from PFO, PSO, and Elovich models, along with correlation coefficients, are listed in Table 2. The R^2 of the PFO model (0.9931) was higher than that of the PSO (0.9631) and Elovich (0.9123) models. Moreover, the calculated q_e of the PFO model (71.79 mg/g) was consistent with the

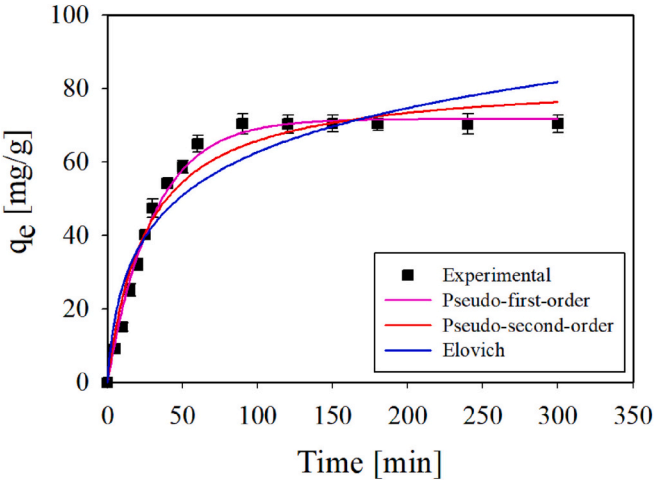

Fig. 9. Non-linear kinetic plots for the adsorption of MB onto Fe_3O_4-GLP@CAB at 25 mg/L.

experimental q_e (70.43 mg/g), but the calculated q_e of the PSO model (82.99 mg/g) was not in accordance with the experimental data. The higher R^2, lower SSE, and χ^2 values confirmed that the PFO model is the most fitted kinetic model to define the sorption mechanism of MB onto Fe_3O_4-GLP@CAB.

3.4. Adsorption isotherms

Isotherm analysis is an essential adsorption model for evaluating the interaction between adsorbate and adsorbent, analyzing the sorption process, and calculating the adsorbent's adsorption capacity. This study explored the batch adsorption results using Freundlich, Langmuir, and D-R (Dubinin-Radushkevich) isotherm models at various temperatures.

Table 2
Kinetic parameters for the adsorption of MB on Fe_3O_4-GLP@CAB at 25 mg/L.

Kinetic model	Parameters	Values
Experimental	$q_{e,\ exp}$ (mg/g)	70.43
Pseudo-first-order	$q_{e1,\ cal}$ (mg/g)	71.79
	k_1 (1/min)	0.0328
	R^2	0.9931
	χ^2	5.45
	SSE	2.28
Pseudo-second-order	$q_{e2,\ cal}$ (mg/g)	82.99
	k_2 (g/mg min)	0.0005
	R^2	0.9631
	χ^2	14.49
	SSE	6.752
Elovich	α (mg/g min)	5.9082
	β (g/mg)	0.0564
	R^2	0.9123
	χ^2	26.69
	SSE	11.585

The Langmuir isotherm describes monolayer sorption on a homogenous surface. It is likewise based on the premise that the adsorption energy is the same at all surface points and that there is no interaction between the adsorbate molecules adhering to the surface. The non-linear form of the Langmuir model can be defined as:

$$q_e = \frac{q_{max} K_L C_e}{1 + K_L C_e} \tag{9}$$

where q_e (mg/g) is the sorption uptake at equilibrium, q_{max} (mg/g) is the sorption uptake, C_e (mg/L) is the equilibrium dye concentration, and K_L (L/mg) is the Langmuir constant. According to data obtained from experiments, the q_{max} decreased (136.7 to 116.2 mg/g) with raising solution temperature (298 to 338 K), suggesting that the adsorption of MB by Fe_3O_4-GLP@CAB was exothermic (i.e., the MB – Fe_3O_4-GLP@CAB interaction was more energetic at low temperature).

The feasibility of adsorption can also be obtained from the fundamental characteristics of the Langmuir isotherms by a dimensionless equilibrium R_L (separation factor), which is described by the following equation:

$$R_L = 1/(1 + K_L C_o) \tag{10}$$

The R_L is used to evaluate the adsorption behavior of adsorbate on the adsorbent, where $R_L = 0$, $R_L > 1$, $R_L = 1.0$, $0 < R_L < 1.0$, and R_L signify irreversible, unfavourable, linear, and favourable adsorption, respectively [53]. The obtained R_L values (Table 3) were within the range of 0 to 1 at different temperatures, confirming the favorability of MB's adsorption onto Fe_3O_4-GLP@CAB.

The Freundlich isotherm model presupposes that sorption takes place on a heterogeneous surface with interactions between molecules that have been adsorbed. The adsorption may be used for multilayer adsorption since it is not limited to the generation of monolayer adsorption. Additionally, this model contends that when the adsorption process is complete, adsorption energy does not remain constant but instead drops exponentially. The non-linear form of the Freundlich equation is expressed as follows:

$$q_e = K_f C_e^{1/n} \tag{11}$$

where K_f (mg/g) is the Freundlich constant refers to the sorption uptake, and n is the sorption intensity (strength). The reduction in K_f values with rising temperature demonstrated that the MB adsorption onto Fe_3O_4-GLP@CAB was exothermic. The values and magnitude of n indicate the adsorption favourability. The values of $n = 1.0$, $n < 1.0$, and $n > 1.0$ indicate a linear, chemical-unfavourable, and physical-favourable process of adsorption [52,54], respectively. The n values (3.672–3.169) were >1 at all temperatures, which implies the physical and favourable adsorption process.

The D-R isotherm model is generally applied to express the sorption mechanism and estimate the adsorbent's porosity properties and the adsorption's apparent energy. The non-linear form of the D-R model is as follows:

$$q_e = q_m exp\left(-\beta\varepsilon^2\right) \tag{12}$$

where q_e (mg/g) and q_m (mg/g) signify the equilibrium and maximal adsorption uptake, respectively. ε is the Polanyi potential and β (mol^2/J^2) is the activity coefficient. The ε value was calculated as follows:

$$\varepsilon = RTln\left(1 + \frac{1}{C_e}\right) \tag{13}$$

where C_e (mg/L) is the dye concentration at equilibrium, R is the gas constant, and T is the ambient temperature. When an adsorbate molecule is brought to the surface of a solid from infinity in a solution, the constant β gives the mean free energy E (kJ/mol) of adsorption per molecule, which can be calculated using the relationship.

$$E = 1\Big/\sqrt{2\beta} \tag{14}$$

The magnitude of E can predict the mechanism of the sorption reaction. If the E value is <8.0 kJ/mol, 8.0–16.0 kJ/mol, and > 16.0 kJ/mol, then the sorption process takes place by physisorption, ion-exchange process, and chemisorption [55], respectively. The calculated E values (Table 4) were <8.0 kJ/mol at various temperatures, which means that the adsorption of MB by Fe_3O_4-GLP@CAB proceeded via a physisorption mechanism.

The plots of the non-linear equation of the D-R, Freundlich, and Langmuir isotherm models at various temperatures are illustrated in Fig. 10, and all parameters, together with correlation coefficients, R^2, SSE, and χ^2, are given in Table 4. According to Table 4, lower χ^2, SSE, and higher R^2 values show that the Langmuir model is the best match compared to the D-R and Freundlich models. As a result, the Langmuir model may represent MB adsorption, indicating that MB molecules are adsorbed on homogeneous sites of the Fe_3O_4-GLP@CAB surface, resulting in monolayer adsorption.

Table 3
Dimensionless constant separation factor (R_L) values at different initial concentrations.

Initial MB concentration (mg/L)	R_L values at different temperatures [K]			
	298	308	318	328
25	0.22	0.265	0.313	0.385
50	0.12	0.153	0.185	0.238
75	0.084	0.107	0.132	0.172
100	0.064	0.083	0.102	0.135
125	0.052	0.067	0.083	0.111
175	0.038	0.049	0.061	0.082
250	0.027	0.035	0.043	0.059

3.5. Comprehensive comparison

A comparison between the maximum adsorption efficiency of Fe_3O_4-GLP@CAB in this study to those of other materials in the literature [56–69] is provided in Table 5. Fe_3O_4-GLP@CAB showed superior performance to other adsorbents, indicating that it is a promising material for removing MB from liquid media.

3.6. Effect of temperature and thermodynamics

Temperature is another crucial component that influences the adsorption behavior [70]. It influences dye molecule diffusion at the interface of the adsorbent's outer boundary layer and dye molecule diffusion inside adsorbent pores. The adsorption process may be endothermic or exothermic, considering the type of dyes and adsorbent. The

Table 4
Isotherm parameters for the adsorption of MB on Fe_3O_4-GLP@CAB at different temperatures.

Isotherm model	Parameters	Temperature (K)			
		298	308	318	328
Langmuir	q_{max} (mg/g)	136.7	131.2	122.7	116.2
	K_L (L/mg)	0.1460	0.111	0.088	0.064
	R^2	0.9984	0.9969	0.9943	0.9941
	χ^2	4.2	6.9	10.7	9.4
	SSE	2.04	2.94	3.87	4.058
Freundlich	K_f (mg/g)	38.78	33.18	28.92	23.29
	n	3.672	3.473	3.414	3.169
	R^2	0.9496	0.9372	0.9254	0.9293
	χ^2	127.97	140.7	130.9	112.4
	SSE	19.31	33.86	24.85	13.59
Dubinin-Radushkevich	q_s (mg/g)	113.77	106.84	101.78	93.92
	K (mol^2/J^2)	0.011	0.035	0.057	0.081
	E (kJ/mol)	6.76	3.77	2.96	2.49
	R^2	0.8319	0.8679	0.8994	0.8957
	χ^2	309.78	210.76	161.9	182.6
	SSE	88.56	57.82	36.63	47.68

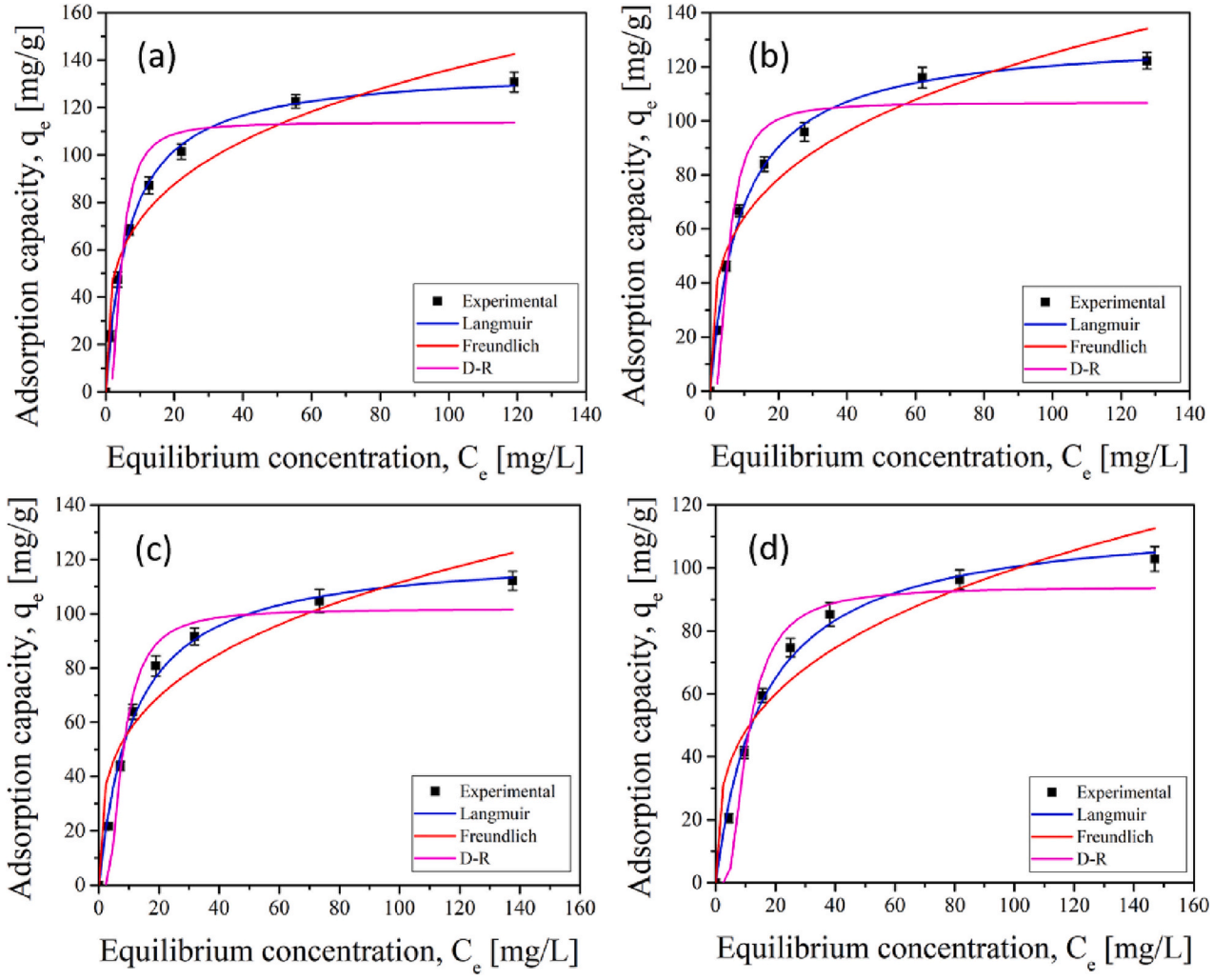

Fig. 10. Non-linear fitting of adsorption isotherms at different temperatures (a) 298 K, (b) 308 K, (c) 318 K, (d) 328 K.

adsorption effectiveness of Fe_3O_4-GLP@CAB on MB in solution was examined in this study at four different temperatures. As shown in Fig. 8f, the removal percentage decreases from 95.1 to 82.4 % with the rise of temperature from 298 to 328 K, which indicates that the adsorption of MB onto Fe_3O_4-GLP@CAB is exothermic. The reduction in removal efficiency with a rise the temperature can be due to the reduction of surface activity and weakening of the physical forces between the MB molecules and Fe_3O_4-GLP@CAB with increasing temperature [71]. Hence, 298 K was chosen as the optimum solution temperature.

The thermodynamic study was performed to gain detailed information regarding MB adsorption onto Fe_3O_4-GLP@CAB further to

Table 5
Comparison of the maximum adsorption uptake of other materials for MB adsorption.

Adsorbent	pH	Dosage (g)	Initial dye concentration (mg/L)	Time (min)	q_{max} (mg/g)	Reference
Zeolite/ferrite nickel/alginate nanocomposite	8.0	0.025	10–50	120	54.05	[56]
Magnetic carbonaceous	–	1.0	51.2–510.36	500	163.93	[57]
ACSO/Fe_3O_4	7.0	0.15	10–100	50	60.6	[58]
Fe-modified banana peel	–	2.5	5–20	50	28.1	[59]
Fe_3O_4 loaded biochar	6.0	0.6	25–200	240	156.4	[60]
Coconut leaves	8.0	1.5	20–100	90	87.82	[61]
mCMNPs	10.0	0.01	5–80	100	37.52	[62]
G-Fe_3O_4/CA	9.0	0.025	10–50	60	51.64	[63]
Ocimum sanctum – Fe_3O_4	7.0	2.5	10–60	60	23.8	[64]
Fe_3O_4@SiO_2-CR	11.0	–	3–27	10	31.44	[65]
Graphene oxide/calcium alginate composite	5.4	0.05	30–80	420	181.8	[66]
Alginate/almond peanut biocomposite	7.0	0.1	10–50	240	22.8	[67]
Clin/Fe_3O_4 (powder form)	10.0	1.0	10–50	60	45.662	[68]
Alginate/Clin/Fe_3O_4 nanocomposite beads	10.0	2.0	10–50	60	12.484	[68]
Magnetic alginate beads	11.0	1.0	20–300	90	106.38	[69]
Magnetic Fe_3O_4 nanoparticles loaded guava leaves powder impregnated into calcium alginate hydrogel beads	10.0	1.0	25–250	90	136.7	Present study

understand the feasibility and mechanism of the sorption process. The thermodynamic factors, like as ΔH^o (enthalpy change), ΔS^o, (entropy change), ΔG^o (Gibbs free energy), and E_a (activation energy) were calculated using the following Eqs.:

$$lnK_d = -[\Delta H^o/RT] + [\Delta S^o/R] \quad (15)$$

$$K_d = \frac{C_o - C_e}{C_e} \quad (16)$$

$$\Delta G^o = -RTlnK_d \quad (17)$$

$$\Delta G^o = \Delta H^o - T\Delta S^o \quad (18)$$

$$\Delta S^o = \frac{\Delta H^o - \Delta G^o}{T} \quad (19)$$

$$ln(1-\theta) = lnA - \frac{E_a}{RT} \quad (20)$$

where R (8.314 J/mol K) is the gas constant, K_d is the distribution coefficient, and T is the temperature of the solution in K. The intercept and slope of the linear plot of 1/T against ln K_d are calculated for calculating the ΔS^o and ΔH^o values (Fig. S2a). The estimated values of thermodynamic factors at various temperatures are listed in Table 6. The adsorption process proceeded spontaneously and grew more hostile with lowering the temperature, according to the negative values of ΔG^o (−7.2999 to −4.0257 kJ/mol), suggesting that increasing temperature was not favourable for adsorption [72–74]. The lower degree of freedom of the deposited MB ions was reflected in the negative ΔS^o value (−106.7 kJ/mol), which also indicated a reduction in the randomness of the solid/liquid interface during the MB ion adsorption process in Fe_3O_4-GLP@CAB [72]. The fact that exothermic nature of the MB adsorption onto Fe_3O_4-GLP@CAB is shown by the negative value of ΔH^o (−38.98 kJ/mol) and the decreasing sorption efficiency with raising the temperature. Additionally, the value of ΔH^o contains details on the adsorption process type. For physisorption, the value of ΔH^o is often between 0 and - 42 kJ/mol, but for chemisorption, the value is generally between −42 and − 125 kJ/mol [75,76]. Therefore, the value of ΔH^o (−38.98 kJ/mol) shows that a physisorption mechanism controls the adsorption process.

Table 6
Thermodynamic parameters for the adsorption of MB on Fe_3O_4-GLP@CAB.

Temperature [K]	ΔG^o (kJ/mol)	ΔS^o (J/mol K)	ΔH^o (kJ/mol)	E_a (kJ/mol)
298	−7.2999			
308	−5.8942	−106.7	−38.98	29.4
318	−5.0887			
328	−4.0257			

The E_a (kJ/mol) was calculated from the slope of the plot of 1/T vs. ln (1-θ) (Fig. S2b). The magnitude of the E_a indicates whether the sorption is primarily chemical or physical. Larger activation energies (40.0–800 kJ/mol) indicate chemisorption, whereas lower activation energies (5.0–40.0 kJ/mol) indicate physisorption [77]. The value of E_a for the removal of MB onto Fe_3O_4-GLP@CAB was determined to be 29.4 kJ/mol, indicating that physisorption was the primary mechanism involved.

3.7. Desorption and reusability studies

Adsorbent regeneration and recovery of valuable adsorbates is an essential part of the adsorption process, which also relates to limiting adsorbent waste. Suppose pollutants can be collected during the desorption process. In that case, they may be used as valuable resources for reuse, lowering the cost of the treatment method after a sufficient number of adsorption-desorption cycles. The reuse of Fe_3O_4-GLP@CAB was investigated by measuring the MB sorption efficiency after treatment with five various eluents. To determine the optimal eluent for MB dye desorption, five different eluents (DI water, 0.2 M HNO_3, 0.2 M NaOH, 0.2 M $(CH_3)_2CO$, and 0.2 M C_2H_5OH) were tested, and the findings are displayed in Fig. S3a. The greatest percentage adsorption of MB under optimum circumstances for fresh Fe_3O_4-GLP@CAB was found to be 95.1 % (control). In Fig. S3a, NaOH and HNO_3 solutions show the lowest (18.4 %) and highest (68.1 %) MB desorption percentages, respectively. The physical nature of the interactions between the Fe_3O_4-GLP@CAB and MB dye may account for the adequate performance of the HNO_3 solution. The presence of H^+ ions in the solution contributes to adsorbent protonation, resulting in electrostatic repulsion between +vely charged sites on the Fe_3O_4-GLP@CAB and cationic MB dye molecules. As a result, the best cationic dye desorbing agents are those that can create more cations in the solution, particularly H^+ ions [78]. The effect of HNO_3 concentrations ranging from 0.2 M to 1.0 M on the untreated Fe_3O_4-GLP@CAB is shown in Fig. S3b. It can be shown that raising the eluent concentrations from 0.2 M to 0.8 M boosted the desorption efficiency. When 0.8 M HNO_3 was utilized as the eluent, the greatest percentage of desorption was determined to be 91.3 %. The higher desorption efficiency might be attributed to the excess of H^+ ions in concentrated HNO_3 solution, causing more dye to desorb from Fe_3O_4-GLP@CAB. However, MB adsorption was somewhat reduced when the Fe_3O_4-GLP@CAB was treated with 1.0 M HNO_3. Fig. S3c shows the

results of a five-cycle cyclic adsorption/regeneration test of the Fe_3O_4-GLP@CAB. After five cycles, the MB dye adsorption decreased marginally from 95.1 % to 78.9 %, showing that HNO_3 successfully regenerated the majority of the sorption sites on the adsorbent. The existence of a proportion of unrecovered sorbed MB molecules that occupied a fraction on the surface of sorption sites explains the reduction in the percentage of MB uptakes. As a result, in terms of reusability, Fe_3O_4-GLP@CAB has a higher possibility for MB removal.

3.8. MB Dye adsorption in real wastewater

The effectiveness of Fe_3O_4-GLP@CAB for MB dye elimination was investigated in water samples taken from various sources such as a river, lake, pond, tap water, and DI water. Adsorption tests were carried out by adding 1.0 g of Fe_3O_4-GLP@CAB to 25 mg/L dye concentrations made using various water samples. The removal efficiency of Fe_3O_4-GLP@CAB for MB dye was found to be somewhat lower in real water samples compared to DI water (Fig. S4). It might be owing to the existence of other frequent competing cationic species in actual water samples, such as Zn^{2+}, Na^{+}, Ca^{2+}, K^{+}, Fe^{3+}, and Mg^{2+}.

3.9. MB dye adsorption mechanism

The adsorption of MB dye is affected by numerous process factors, including pH_{PZC}, solution pH, surface functional groups, and adsorbent porosity. MB adsorbs onto Fe_3O_4-GLP@CAB through liquid-solid phase interaction, which might be pore diffusion, hydrogen bonding, and electrostatic interaction. MB dye may have adsorbed onto the Fe_3O_4-GLP@CAB as following mechanism and interaction:

- MB dye molecules are electrostatically attracted towards the -vely charged Fe_3O_4-GLP@CAB. At pH > pH_{PZC}, the surface of the Fe_3O_4-GLP@CAB was covered with -vely charged —O and -COO^{-} groups which electrically bonded or interacted with +vely charged (N^{+} atoms) groups of MB dye molecules. The possible schemes of MB dye adsorption onto Fe_3O_4-GLP@CAB are given in Fig. 11. This electrostatic interaction made a stronger link between them.
- H-bonding is also involved in the adsorption of MB by Fe_3O_4-GLP@CAB. At pH ≤ pH_{PZC}, the -OH and -COOH groups on the surface of Fe_3O_4-GLP@CAB may be provided H-atoms to commence H-bonding with the polar N-atom of MB (Fig. 11). At basic pH, H-bonding contributes less than electrostatic interaction.
- The Fe_3O_4-GLP@CAB porous structure suggests the possibility of adsorbed MB dye molecules via pore diffusion and the physical process.
- The surface functional groups of the Fe_3O_4-GLP@CAB interacted with the MB dye molecules by electrostatic contact and hydrogen bonding, according to FTIR analyses of the Fe_3O_4-GLP@CAB before and after MB dye adsorption.

4. Conclusions

In this work, novel Fe_3O_4-GLP@CAB was successfully synthesized by a simple and inexpensive method and employed to remove MB from an aqueous solution. Characterization approaches (BET/BJH, FTIR, VSM, FE-SEM/EDX, pH_{PZC}, and XRD) proved the successful incorporation of Fe_3O_4-GLP into the CAB. The Ms. value of the Fe_3O_4-GLP@CAB was 7.8 emu/g, which confirms the high separation capability of the Fe_3O_4-GLP@CAB by a magnet. The MB removal depends on temperature, dosage, solution pH, contact duration, MB dye concentration, and stirring speed. The maximum removal efficiency of MB (95.2 %) on the Fe_3O_4-GLP@CAB occurred at pH = 10.0, dosage = 1.0 g/30 mL, MB dye concentration = 25 mg/L, agitation speed = 250 rpm, contact duration = 90 min, and temperature = 298 K. Considering the values of χ^2, SSE, and R^2, the adsorption of MB on Fe_3O_4-GLP@CAB best fitted to the Langmuir isotherm model. The maximal adsorption efficiency by the Langmuir model is calculated to be 136.7 mg/g at 298 K. As the temperature increased, the adsorption efficiency decreased. PFO kinetic model better described the adsorption kinetics. Various thermodynamic factors were obtained from the adsorption process, revealing that the adsorption process was exothermic. The negative values of ΔS^{o} (−106.7 J/mol K), ΔH^{o} (−38.98 kJ/mol), and ΔG^{o} (−7.2999 to −4.0257 kJ/mol) demonstrate that the adsorption of MB onto Fe_3O_4-GLP@CAB was random, physical, and spontaneous within the experiment

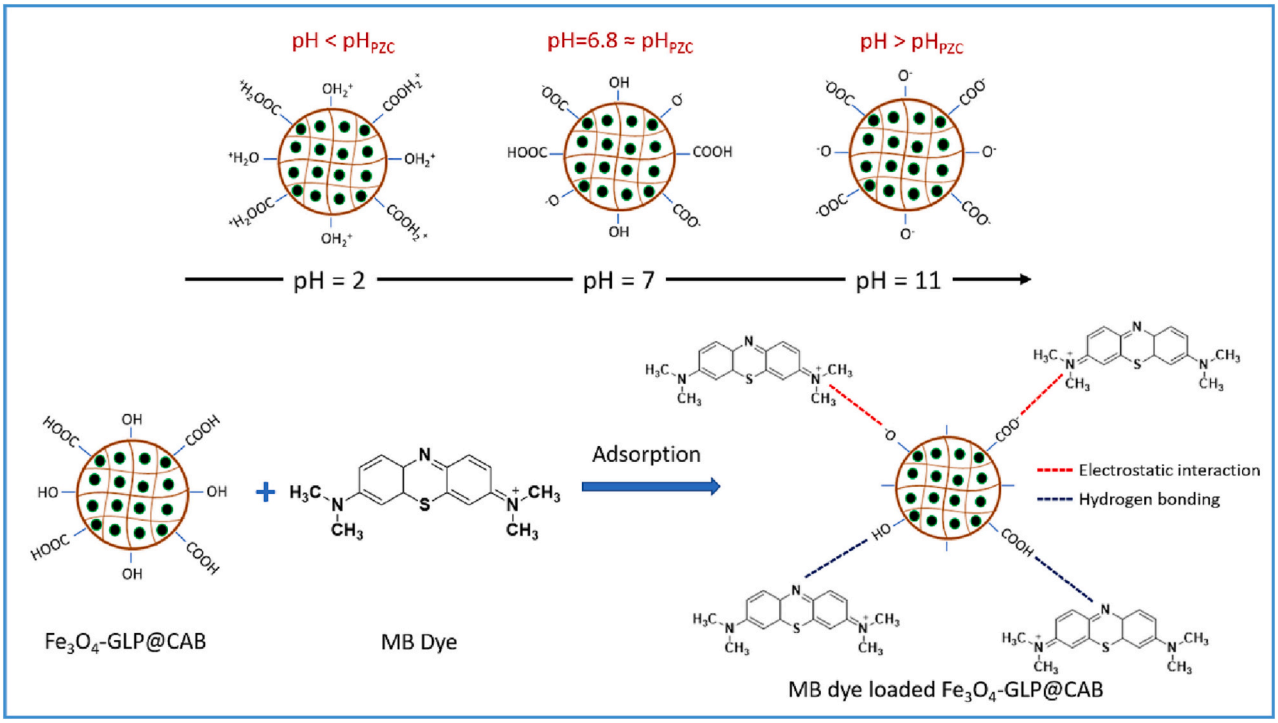

Fig. 11. Possible interaction and mechanism of MB dye adsorption onto Fe_3O_4-GLP@CAB.

temperatures. The adsorption mechanism of MB on Fe_3O_4-GLP@CAB occurred through electrostatic interaction, pore diffusion, hydrogen bonding, and physisorption. Desorption and regeneration of MB could be attained by using 0.8 M HNO_3 eluent, and the recyclability results showed that Fe_3O_4-GLP@CAB was very appropriate for the removal of MB from the liquid phase after five cycles. These results designated that Fe_3O_4-GLP@CAB could be employed as an efficient and environmentally friendly sorbent for the elimination of MB from an aqueous environment.

CRediT authorship contribution statement

Venkata Subbaiah Munagapati: Writing – original draft, Data curation, Methodology, Conceptualization, Visualization, Formal analysis. **Hsin-Yu Wen:** Conceptualization, Validation, Visualization. **Anjani R.K. Gollakota:** Data curation, Formal analysis, Conceptualization. **Jet-Chau Wen:** Conceptualization, Supervision, Resources, Funding acquisition, Data curation, Writing – review & editing. **Kun-Yi Andrew Lin:** Data curation, Visualization, Writing – review & editing. **Chi-Min Shu:** Conceptualization, Writing – review & editing. **Vijaya Yarramuthi:** Data curation, Visualization, Validation. **Praveen Kumar Basivi:** Formal analysis. **Guda Mallikarjuna Reddy:** Conceptualization. **Grigory V. Zyryanov:** Conceptualization.

Declaration of competing interest

The authors declare that they have no known competing financial interests or personal relationships that could have appeared to influence the work reported in this paper.

Acknowledgements

The authors would like to acknowledge the research support from NSTC 110-2625-M-224-001 and 111-2625-M-224-001 by the National Science and Technology Council, Taiwan.

Appendix A. Supplementary data

Supplementary data to this article can be found online at https://doi.org/10.1016/j.ijbiomac.2023.125675.

References

[1] B.R. Patra, S. Nanda, A.K. Dalai, V. Meda, Taguchi-based process optimization for activation of agro-food waste biochar and performance test for dye adsorption, Chemosphere 285 (2021), 131531, https://doi.org/10.1016/j.chemosphere.2021.131531.

[2] P. Kumbhar, D. Narale, R. Bhosale, C. Jambhale, J.H. Kim, S. Kolekar, Synthesis of tea waste/Fe_3O_4 magnetic composite (TWMC) for efficient adsorption of crystal violet dye: isotherm, kinetic and thermodynamic studies, J. Environ. Chem. Eng. 10 (2022), 107893, https://doi.org/10.1016/j.jece.2022.107893.

[3] Y. Li, S. Wang, Z. Shen, X. Li, Q. Zhou, Y. Sun, T. Wang, Y. Liu, Q. Gao, Gradient adsorption of methylene blue and crystal violet onto compound microporous silica from aqueous medium, ACS Omega 5 (2020) 28382–28392, https://doi.org/10.1021/acsomega.0c04437.

[4] P.S. Thue, A.C. Sophia, E.C. Lima, A.G.N. Wamba, W.S. de Alencar, G.S. dos Reis, F. S. Rodembusch, S.L.P. Dias, Synthesis and characterization of a novel organic-inorganic hybrid clay adsorbent for the removal of acid red 1 and acid green 25 from aqueous solutions, J. Clean. Prod. 171 (2018) 30–44, https://doi.org/10.1016/j.jclepro.2017.09.278.

[5] H.D. Bouras, Z. Isik, E. Bezirhan Arikan, N. Bouras, A. Chergui, H.C. Yatmaz, N. Dizge, Photocatalytic oxidation of azo dye solutions by impregnation of ZnO on fungi, Biochem. Eng. J. 146 (2019) 150–159, https://doi.org/10.1016/j.bej.2019.03.014.

[6] B.T. Gemici, H.U. Ozel, H.B. Ozel, Removal of methylene blue onto forest wastes: adsorption isotherms, kinetics and thermodynamic analysis, Environ. Technol. Innov. 22 (2021), 101501, https://doi.org/10.1016/j.eti.2021.101501.

[7] A.M. Aldawsari, I. Alsohaimi, H.M.A. Hassan, Z.E.A. Abdalla, I. Hassan, M. R. Berber, Tailoring an efficient nanocomposite of activated carbon-layered double hydroxide for elimination of water-soluble dyes, J. Alloys Compd. 857 (2021), 157551, https://doi.org/10.1016/j.jallcom.2020.157551.

[8] I.H. Alsohaimi, M.S. Alhumaimess, A.A. Alqadami, G.T. Alshammari, R.F. Al-Olaimi, A.A. Abdeltawab, M.Y. El-Sayed, H.M. Hassan, Adsorptive performance of aminonaphthalenesulfonic acid modified magnetic-graphene oxide for methylene blue dye: mechanism, isotherm and thermodynamic studies, Inorg. Chem. Commun. 147 (2023), 110261, https://doi.org/10.1016/j.inoche.2022.110261.

[9] H.M.A. Hassan, M.R. El-Aassar, M.A. El-Hashemy, M.A. Betiha, M. Alzaid, A. N. Alqhobisi, L.A. Alzarea, I.H. Alsohaimi, Sulfanilic acid-functionalized magnetic GO as a robust adsorbent for the efficient adsorption of methylene blue from aqueous solution, J. Mol. Liq. 361 (2022), 119603, https://doi.org/10.1016/j.molliq.2022.119603.

[10] A.R.K. Gollakota, M.V. Subbaiah, C.-M. Shu, P.K. Sarangi, J.-C. Wen, Polymer functionalized hazel sterculia hydrogel beads for adsorption of anionic azo dye RR120 from industrial streams, Process Saf. Environ. Protect. 175 (2023) 665–676, https://doi.org/10.1016/j.psep.2023.05.083.

[11] Z. Jia, Z. Li, T. Ni, S. Li, Adsorption of low-cost absorption materials based on biomass (Cortaderia selloana flower spikes) for dye removal: kinetics, isotherms and thermodynamic studies, J. Mol. Liq. 229 (2017) 285–292, https://doi.org/10.1016/j.molliq.2016.12.059.

[12] V. Ugraskan, B. Isik, O. Yazici, F. Cakar, Removal of Safranine T by a highly efficient adsorbent (Cotinus Coggygria leaves): isotherms, kinetics, thermodynamics, and surface properties, Surf. Interfaces 28 (2022), 101615, https://doi.org/10.1016/j.surfin.2021.101615.

[13] A. Ouldmoumna, L. Reinert, N. Benderdouche, B. Bestani, L. Duclaux, Characterization and application of three novel biosorbents "Eucalyptus globulus, Cynara cardunculus, and Prunus cerasefera" to dye removal, Desalin. Water Treat. 51 (2013) 3527–3538, https://doi.org/10.1080/19443994.2012.749583.

[14] A. Malhotra, S. Srivastava, S. Manjhu, R.S. Lokhande, R. Sahu, S.K. Jain, K. B. Sharma, B. Tripathi, Study of adsorbent characteristics of palm leaves powder as a bio sorbent for removal of malachite green (MG) dye, Mater. Today Proc. 67 (2022) 900–904, https://doi.org/10.1016/j.matpr.2022.07.347.

[15] R. Zein, J.S. Purnomo, P. Ramadhani, M.F. Alif, S. Safni, Lemongrass (Cymbopogon nardus) leaves biowaste as an effective and low-cost adsorbent for methylene blue dyes removal: isotherms, kinetics, and thermodynamics studies, Sep. Sci. Technol. 57 (2022) 2341–2357, https://doi.org/10.1080/01496395.2022.2058549.

[16] N. Gupta, A.K. Kushwaha, M.C. Chattopadhyaya, Application of potato (Solanum tuberosum) plant wastes for the removal of methylene blue and malachite green dye from aqueous solution, Arab. J. Chem. 9 (2016) S707–S716, https://doi.org/10.1016/j.arabjc.2011.07.021.

[17] G.D. Arend, L.S. Soares, C. Camelo-Silva, M.A.R. Sanches, F.M. Penha, E. Díaz-De-Cerio, V. Verardo, E.S. Prudencio, A. Segura-Carretero, B. Tischer, J.C. Cunha Petrus, S. Verruck, K. Rezzadori, Is nanofiltration an efficient technology to recover and stabilize phenolic compounds from guava (Psidium guajava) leaves extract? Food Biosci. 50 (2022), 101997 https://doi.org/10.1016/j.fbio.2022.101997.

[18] M. Touihri, F. Guesmi, C. Hannachi, B. Hamrouni, L. Sellaoui, M. Badawi, J. Poch, N. Fiol, Single and simultaneous adsorption of Cr(VI) and Cu (II) on a novel Fe_3O_4/pine cones gel beads nanocomposite: experiments, characterization and isotherms modeling, Chem. Eng. J. 416 (2021), 129101, https://doi.org/10.1016/j.cej.2021.129101.

[19] A. Pholosi, E.B. Naidoo, A.E. Ofomaja, Intraparticle diffusion of Cr(VI) through biomass and magnetite coated biomass: a comparative kinetic and diffusion study, S. Afr. J. Chem. Eng. 32 (2020) 39–55, https://doi.org/10.1016/j.sajce.2020.01.005.

[20] S. Sadeghi, F.A. Rad, A.Z. Moghaddam, A highly selective sorbent for removal of Cr (VI) from aqueous solutions based on Fe3O4/poly(methyl methacrylate) grafted Tragacanth gum nanocomposite: optimization by experimental design, Mater. Sci. Eng. C 45 (2014) 136–145, https://doi.org/10.1016/j.msec.2014.08.063.

[21] A.I. Adeogun, J.A. Akande, M.A. Idowu, S.O. Kareem, Magnetic tuned sorghum husk biosorbent for effective removal of cationic dyes from aqueous solution: isotherm, kinetics, thermodynamics and optimization studies, Appl Water Sci 9 (2019) 160, https://doi.org/10.1007/s13201-019-1037-2.

[22] J. Geng, J. Chang, Synthesis of magnetic Forsythia suspensa leaf powders for removal of metal ions and dyes from wastewater, J. Environ. Chem. Eng. 8 (2020), 104224, https://doi.org/10.1016/j.jece.2020.104224.

[23] V. Subbaiah Munagapati, H.Y. Wen, A.R.K. Gollakota, J.C. Wen, C.M. Shu, K. Y. Andrew Lin, Z. Tian, J.H. Wen, G. Mallikarjuna Reddy, G.V. Zyryanov, Magnetic Fe_3O_4 nanoparticles loaded papaya (Carica papaya L.) seed powder as an effective and recyclable adsorbent material for the separation of anionic azo dye (Congo Red) from liquid phase: Evaluation of adsorption properties, J. Mol. Liq. 345 (2022), 118255, https://doi.org/10.1016/j.molliq.2021.118255.

[24] A. Mohammadifard, D. Allouss, M. Vosoughi, A. Dargahi, A. Moharrami, Synthesis of magnetic Fe_3O_4/activated carbon prepared from banana peel (BPAC@Fe_3O_4) and salvia seed (SSAC@Fe_3O_4) and applications in the adsorption of Basic Blue 41 textile dye from aqueous solutions, Appl Water Sci 12 (2022) 88, https://doi.org/10.1007/s13201-022-01622-6.

[25] K. Narasimharao, S. Al-Thabaiti, H.K. Rajor, M. Mokhtar, A. Alsheshri, S.Y. Alfaifi, S.I. Siddiqui, N.K. Abdulla, Fe_3O_4@date seeds powder: a sustainable nanocomposite material for wastewater treatment, J. Mater. Res. Technol. 18 (2022) 3581–3597, https://doi.org/10.1016/j.jmrt.2022.03.176.

[26] N. Boukhalfa, M. Boutahala, N. Djebri, A. Idris, Kinetics, thermodynamics, equilibrium isotherms, and reusability studies of cationic dye adsorption by magnetic alginate/oxidized multiwalled carbon nanotubes composites, Int. J. Biol. Macromol. 123 (2019) 539–548, https://doi.org/10.1016/j.ijbiomac.2018.11.102.

[27] N. Djebri, M. Boutahala, N.E. Chelali, N. Boukhalfa, L. Zeroual, Enhanced removal of cationic dye by calcium alginate/organobentonite beads: modeling, kinetics, equilibriums, thermodynamic and reusability studies, Int. J. Biol. Macromol. 92 (2016) 1277–1287, https://doi.org/10.1016/j.ijbiomac.2016.08.013.

[28] S. Yadav, A. Asthana, A.K. Singh, R. Chakraborty, S.S. Vidya, M.A.B.H. Susan, S.A. C. Carabineiro, Adsorption of cationic dyes, drugs and metal from aqueous

solutions using a polymer composite of magnetic/β-cyclodextrin/activated charcoal/Na alginate: isotherm, kinetics and regeneration studies, J. Hazard. Mater. 409 (2021), 124840, https://doi.org/10.1016/j.jhazmat.2020.124840.
[29] R. Soury, M. Jabli, S. Latif, K.M. Alenezi, M. El Oudi, F. Abdulaziz, S. Teka, H. El Moll, A. Haque, Synthesis and characterization of a new meso-tetrakis (2,4,6-trimethylphenyl) porphyrinto) zinc(II) supported sodium alginate gel beads for improved adsorption of methylene blue dye, Int. J. Biol. Macromol. 202 (2022) 161–176, https://doi.org/10.1016/j.ijbiomac.2022.01.087.
[30] W. Jaihan, V. Mohdee, S. Sanongraj, U. Pancharoen, K. Nootong, Biosorption of lead (II) from aqueous solution using cellulose-based bio-adsorbents prepared from unripe papaya (Carica papaya) peel waste: removal efficiency, thermodynamics, kinetics and isotherm analysis: biosorption of lead (II) from aqueous solution, Arab. J. Chem. 15 (2022), 103883, https://doi.org/10.1016/j.arabjc.2022.103883.
[31] T. Altalhi, A.A. El-moemen, M.M. Ibrahim, A. Mezni, I.H. Alsohaimi, M.H. H. Mahmoud, T. Kumeria, G.A.M. Mersal, N.Y. Mostafa, Integrated approach in treatment of solid olive residue and olive wastewater, Mater. Res. Express 8 (2021), 115503, https://doi.org/10.1088/2053-1591/ac34b9.
[32] S. Zhou, L. Xia, Z. Fu, C. Zhang, X. Duan, S. Zhang, Y. Wang, C. Ding, X. Liu, W. Xu, Purification of dye-contaminated ethanol-water mixture using magnetic cellulose powders derived from agricultural waste biomass, Carbohydr. Polym. 258 (2021), 117690, https://doi.org/10.1016/j.carbpol.2021.117690.
[33] N.J. Khound, R.K. Bharali, Biosorption of fluoride from aqueous medium by Indian sandalwood (Santalum Album) leaf powder, J. Environ. Chem. Eng. 6 (2018) 1726–1735, https://doi.org/10.1016/j.jece.2018.02.010.
[34] A.M. Aldawsari, H.M.A. Hassan, A.N. Alrashidi, I.H. Alsohaimi, S.M.N. Moustafa, H.M. Youssef, R. Hamdi, M.A. Azzam, Preparation of PVDF-co-PAAm membrane with robust antifouling, and antibacterial performance by blending with magnetic graphene oxide, J. Environ. Chem. Eng. 10 (2022), 108093, https://doi.org/10.1016/j.jece.2022.108093.
[35] Y. Zheng, J. Wang, D. Li, C. Liu, Y. Lu, X. Lin, Z. Zheng, Insight into the KOH/$KMnO_4$ activation mechanism of oxygen-enriched hierarchical porous biochar derived from biomass waste by in-situ pyrolysis for methylene blue enhanced adsorption, J. Anal. Appl. Pyrolysis 158 (2021), 105269, https://doi.org/10.1016/j.jaap.2021.105269.
[36] E. Alver, A.Ü. Metin, F. Brouers, Methylene blue adsorption on magnetic alginate/rice husk bio-composite, Int. J. Biol. Macromol. 154 (2020) 104–113, https://doi.org/10.1016/j.ijbiomac.2020.02.330.
[37] K. Akin, V. Ugraskan, B. Isik, F. Cakar, Adsorptive removal of crystal violet from wastewater using sodium alginate-gelatin-montmorillonite ternary composite microbeads, Int. J. Biol. Macromol. 223 (2022) 543–554, https://doi.org/10.1016/j.ijbiomac.2022.11.002.
[38] H. Daemi, M. Barikani, Synthesis and characterization of calcium alginate nanoparticles, sodium homopolymannuronate salt and its calcium nanoparticles, Sci. Iran. 19 (2012) 2023–2028, https://doi.org/10.1016/j.scient.2012.10.005.
[39] H. Zhu, S. Chen, H. Duan, J. He, Y. Luo, Removal of anionic and cationic dyes using porous chitosan/carboxymethyl cellulose-PEG hydrogels: optimization, adsorption kinetics, isotherm and thermodynamics studies, Int. J. Biol. Macromol. 231 (2023), 123213, https://doi.org/10.1016/j.ijbiomac.2023.123213.
[40] J. Feng, J. Zhang, W. Song, J. Liu, Z. Hu, B. Bao, An environmental-friendly magnetic bio-adsorbent for high-efficiency Pb(II) removal: preparation, characterization and its adsorption performance, Ecotoxicol. Environ. Saf. 203 (2020), 111002, https://doi.org/10.1016/j.ecoenv.2020.111002.
[41] J.N. Edokpayi, E. Makete, Removal of Congo red dye from aqueous media using Litchi seeds powder: equilibrium, kinetics and thermodynamics, Phys. Chem. Earth 123 (2021), 103007, https://doi.org/10.1016/j.pce.2021.103007.
[42] S. Ben Ayed, L. Mansour, V. Vaiano, A. Halim Harrath, F. Ayari, L. Rizzo, Magnetic Fe_3O_4-natural iron ore/calcium alginate beads as heterogeneous catalyst for Novacron blue dye degradation in water by (photo)Fenton process, J. Photochem. Photobiol. A Chem. 438 (2023), 114566, https://doi.org/10.1016/j.jphotochem.2023.114566.
[43] M. Askarieh, H. Farshidi, A. Rashidi, A. Pourreza, M.S. Alivand, Comparative evaluation of MIL-101(Cr)/calcium alginate composite beads as potential adsorbents for removing water vapor from air, Sep. Purif. Technol. 291 (2022), 120830, https://doi.org/10.1016/j.seppur.2022.120830.
[44] K.G. Akpomie, J. Conradie, Biosorption and regeneration potentials of magnetite nanoparticle loaded Solanum tuberosum peel for celestine blue dye, Int. J. Phytorem. 23 (2021) 347–361, https://doi.org/10.1080/15226514.2020.1814198.
[45] A.R.D. Ahmad, S.S. Imam, R. Adnan, W. Da Oh, A.F. Abdul Latip, A.A.D. Ahmad, Fenton degradation of ofloxacin antibiotic using calcium alginate beads impregnated with Fe_3O_4-montmorillonite composite, Int. J. Biol. Macromol. 229 (2023) 838–848, https://doi.org/10.1016/j.ijbiomac.2022.12.287.
[46] M. Loutfi, R. Mariouch, I. Mariouch, M. Belfaquir, M.S. ElYoubi, Adsorption of methylene blue dye from aqueous solutions onto natural clay: equilibrium and kinetic studies, Mater. Today Proc. 72 (2023) 3638–3643, https://doi.org/10.1016/j.matpr.2022.08.412.
[47] T.F. de Oliveira, C.P. de Souza, A.L. Lopes-Moriyama, M.L. Pereira da Silva, In situ modification of MCM-41 using niobium and tantalum mixed oxide from columbite processing for methylene blue adsorption: characterization, kinetic, isotherm, thermodynamic and mechanism study, Mater. Chem. Phys. 294 (2023), 127011, https://doi.org/10.1016/j.matchemphys.2022.127011.
[48] S.T. Nipa, N.R. Shefa, S. Parvin, M.A. Khatun, M.J. Alam, S. Chowdhury, M.A. R. Khan, S.M.A.Z. Shawon, B.K. Biswas, M.W. Rahman, Adsorption of methylene blue on papaya bark fiber: equilibrium, isotherm and kinetic perspectives, Results Eng. 17 (2023), 100857, https://doi.org/10.1016/j.rineng.2022.100857.
[49] D. Brahma, H. Saikia, Synthesis of ZrO_2/MgAl-LDH composites and evaluation of its isotherm, kinetics and thermodynamic properties in the adsorption of Congo red dye, Chem. Thermodyn. Therm. Anal. 7 (2022), 100067, https://doi.org/10.1016/j.ctta.2022.100067.
[50] S. Sahu, S. Pahi, S. Tripathy, S.K. Singh, A. Behera, U.K. Sahu, R.K. Patel, Adsorption of methylene blue on chemically modified lychee seed biochar: dynamic, equilibrium, and thermodynamic study, J. Mol. Liq. 315 (2020), 113743, https://doi.org/10.1016/j.molliq.2020.113743.
[51] N.C. Thanh, S. Shanmugam, S. Shanmugasundaram, M.S. AlSalhi, S. Devanesan, R. Shanmuganathan, N.T. Lan Chi, Comparison of Simarouba glauca seed shell carbons for enhanced direct red 12B dye adsorption: adsorption isotherm and kinetic studies, Food Chem. Toxicol. 168 (2022), 113326, https://doi.org/10.1016/j.fct.2022.113326.
[52] M. Maqbool, S. Sadaf, H.N. Bhatti, S. Rehmat, A. Kausar, S.A. Alissa, M. Iqbal, Sodium alginate and polypyrrole composites with algal dead biomass for the adsorption of Congo red dye: kinetics, thermodynamics and desorption studies, Surf. Interfaces 25 (2021), 101183, https://doi.org/10.1016/j.surfin.2021.101183.
[53] I. Apostol, N. Anghel, F. Doroftei, A. Bele, I. Spiridon, Xanthan or esterified xanthan/cobalt ferrite-lignin hybrid materials for methyl blue and basic fuchsine dyes removal: equilibrium, kinetic and thermodynamic studies, Mater. Today Chem. 27 (2023), 101299, https://doi.org/10.1016/j.mtchem.2022.101299.
[54] N. Kumar, J. Kaur, V. Kumar, S. Preet, R. Kumar, Synthesis and dye adsorption studies of WO_3/MoO_3 nanocomposites, J. Phys. Chem. Solids 174 (2023), 111179, https://doi.org/10.1016/j.jpcs.2022.111179.
[55] S. Archana, B.K. Jayanna, A. Ananda, M.S. Ananth, A. Mossad Ali, H. B. Muralidhara, K.Y. Kumar, Numerical investigations of response surface methodology for organic dye adsorption onto mg-Al LDH-GO nano hybrid: an optimization, kinetics and isothermal studies, J. Indian Chem. Soc. 99 (2022), 100249, https://doi.org/10.1016/j.jics.2021.100249.
[56] M. Bayat, V. Javanbakht, J. Esmaili, Synthesis of zeolite/nickel ferrite/sodium alginate bionanocomposite via a co-precipitation technique for efficient removal of water-soluble methylene blue dye, Int. J. Biol. Macromol. 116 (2018) 607–619, https://doi.org/10.1016/j.ijbiomac.2018.05.012.
[57] H. Ma, J.B. Li, W.W. Liu, M. Miao, B.J. Cheng, S.W. Zhu, Novel synthesis of a versatile magnetic adsorbent derived from corncob for dye removal, Bioresour. Technol. 190 (2015) 13–20, https://doi.org/10.1016/j.biortech.2015.04.048.
[58] R. Foroutan, R. Mohammadi, J. Razeghi, B. Ramavandi, Performance of algal activated carbon/Fe_3O_4 magnetic composite for cationic dyes removal from aqueous solutions, Algal Res. 40 (2019), 101509, https://doi.org/10.1016/j.algal.2019.101509.
[59] F. Çatlıoğlu, S. Akay, E. Turunç, B. Gözmen, I. Anastopoulos, B. Kayan, D. Kalderis, Preparation and application of Fe-modified banana peel in the adsorption of methylene blue: process optimization using response surface methodology, Environ. Nanotechnol. Monit. Manag. 16 (2021), 100517, https://doi.org/10.1016/j.enmm.2021.100517.
[60] J. Xie, R. Lin, Z. Liang, Z. Zhao, C. Yang, F. Cui, Effect of cations on the enhanced adsorption of cationic dye in Fe_3O_4-loaded biochar and mechanism, J. Environ. Chem. Eng. 9 (2021), 105744, https://doi.org/10.1016/j.jece.2021.105744.
[61] A.H. Jawad, M.A.M. Ishak, A.M. Farhan, K. Ismail, Response surface methodology approach for optimization of color removal and COD reduction of methylene blue using microwave-induced NaOH activated carbon from biomass waste, Desalin. Water Treat. 62 (2017) 208–220, https://doi.org/10.5004/dwt.2017.20132.
[62] Y. Lei, X. Zhang, X. Meng, Z. Wang, The preparation of core–shell Fe_3O_4@SiO2 magnetic nanoparticles with different surface carboxyl densities and their application in the removal of methylene blue, Inorg. Chem. Commun. 139 (2022), 109381, https://doi.org/10.1016/j.inoche.2022.109381.
[63] N. Song, X.L. Wu, S. Zhong, H. Lin, J.R. Chen, Biocompatible G-Fe_3O_4/CA nanocomposites for the removal of methylene blue, J. Mol. Liq. 212 (2015) 63–69, https://doi.org/10.1016/j.molliq.2015.08.059.
[64] A. Sharma, D. Mangla, A. Choudhry, M. Sajid, S. Ali Chaudhry, Facile synthesis, physico-chemical studies of Ocimum sanctum magnetic nanocomposite and its adsorptive application against methylene blue, J. Mol. Liq. 362 (2022), 119752, https://doi.org/10.1016/j.molliq.2022.119752.
[65] D. Yimin, Z. Jiaqi, L. Danyang, N. Lanli, Z. Liling, Z. Yi, Z. Xiaohong, Preparation of Congo red functionalized Fe_3O_4@SiO_2 nanoparticle and its application for the removal of methylene blue, Colloids Surf. A Physicochem. Eng. Asp. 550 (2018) 90–98, https://doi.org/10.1016/j.colsurfa.2018.04.033.
[66] Y. Li, Q. Du, T. Liu, J. Sun, Y. Wang, S. Wu, Z. Wang, Y. Xia, L. Xia, Methylene blue adsorption on graphene oxide/calcium alginate composites, Carbohydr. Polym. 95 (2013) 501–507, https://doi.org/10.1016/j.carbpol.2013.01.094.
[67] M. Erfani, V. Javanbakht, Methylene Blue removal from aqueous solution by a biocomposite synthesized from sodium alginate and wastes of oil extraction from almond peanut, Int. J. Biol. Macromol. 114 (2018) 244–255, https://doi.org/10.1016/j.ijbiomac.2018.03.003.
[68] M. Noori, M. Tahmasebpoor, R. Foroutan, Enhanced adsorption capacity of low-cost magnetic clinoptilolite powders/beads for the effective removal of methylene blue: adsorption and desorption studies, Mater. Chem. Phys. 278 (2022), 125655, https://doi.org/10.1016/j.matchemphys.2021.125655.
[69] H. Rezaei, M. Haghshenasfard, A. Moheb, Optimization of dye adsorption using Fe_3O_4 nanoparticles encapsulated with alginate beads by Taguchi method, Adsorpt. Sci. Technol. 35 (2017) 55–71, https://doi.org/10.1177/0263617416667508.
[70] M.S. Alshammari, I.M. Ahmed, J.S. Alsharari, I.H. Alsohaimi, N.S. Al-Muaikel, T. S. Alraddadi, T.H.A. Hasanin, Adsorption of Cr(VI) using α-Fe_2O_3 coated hydroxy magnesium silicate (HMS): isotherm, thermodynamic and kinetic study, Int. J.

Environ. Anal. Chem. 103 (2023) 2223–2239, https://doi.org/10.1080/03067319.2021.1890061.

[71] I. Hotan Alsohaimi, M.S. Alhumaimess, A. Abdullah Alqadami, G. Tharwi Alshammari, R. Fawzy Al-Olaimi, A.A. Abdeltawab, M.Y. El-Sayed, H.M. Hassan, Adsorptive performance of aminonaphthalenesulfonic acid modified magnetic-graphene oxide for methylene blue dye: mechanism, isotherm and thermodynamic studies, Inorg. Chem. Commun. 147 (2023), 110261, https://doi.org/10.1016/j.inoche.2022.110261.

[72] M.X. Xiong, M. Yang, Q.L. Chen, T.Y. Cai, Mechanism studies for adsorption and extraction of soluble sodium from bauxite residue: characterization, kinetics, and thermodynamics, J. Environ. Chem. Eng. 10 (2022), 108183, https://doi.org/10.1016/j.jece.2022.108183.

[73] A.M. Aldawsari, I.H. Alsohaimi, A.A. Al-Kahtani, A.A. Alqadami, Z.E.A. Abdalla, E. A. Musad Saleh, Adsorptive performance of aminoterephthalic acid modified oxidized activated carbon for malachite green dye: mechanism, kinetic and thermodynamic studies, Sep. Sci. Technol. 56 (2021) 835–846, https://doi.org/10.1080/01496395.2020.1737121.

[74] E.H. Alosaimi, I.H. Alsohaimi, T.E. Dahan, Q. Chen, S. Melhi, Adsorptive performance of tetracarboxylic acid-modified magnetic silica nanocomposite for recoverable efficient removal of toxic Cd(II) from aqueous environment: equilibrium, isotherm, and reusability studies, J. Mol. Liq. 334 (2021), 116069, https://doi.org/10.1016/j.molliq.2021.116069.

[75] L. Zhou, S. Pan, X. Chen, Y. Zhao, B. Zou, M. Jin, Kinetics and thermodynamics studies of pentachlorophenol adsorption on covalently functionalized Fe_3O_4@SiO_2-MWCNTs core-shell magnetic microspheres, Chem. Eng. J. 257 (2014) 10–19, https://doi.org/10.1016/j.cej.2014.07.060.

[76] A.M. Aldawsari, I.H. Alsohaimi, H.M.A. Hassan, M.R. Berber, Z.E.A. Abdalla, I. Hassan, E.A. Musad Saleh, B.H. Hameed, Activated carbon/MOFs composite: AC/NH_2-MIL-101(Cr), synthesis and application in high performance adsorption of p-nitrophenol, J. Saudi Chem. Soc. 24 (2020) 693–703, https://doi.org/10.1016/j.jscs.2020.07.009.

[77] H.R. Mahmoud, S.M. Ibrahim, S.A. El-Molla, Textile dye removal from aqueous solutions using cheap MgO nanomaterials: adsorption kinetics, isotherm studies and thermodynamics, Adv. Powder Technol. 27 (2016) 223–231, https://doi.org/10.1016/j.apt.2015.12.006.

[78] E. Daneshvar, A. Vazirzadeh, A. Niazi, M. Kousha, M. Naushad, A. Bhatnagar, Desorption of methylene blue dye from brown macroalga: effects of operating parameters, isotherm study and kinetic modeling, J. Clean. Prod. 152 (2017) 443–453, https://doi.org/10.1016/j.jclepro.2017.03.119.